polyclonal antibody (Santa Cruz Biotechnology) followed by an Alexa Flour 488 donkey anti-rabbit IgG (H + L) (Invitrogen, Carlsbad, CA, USA). These foci were observed under a BIOREVO BZ-9000 microscope (Keyence, Osaka, Japan).

Neutral comet assays. Neutral comet assays were performed using the CometAssay kit (Trevigen, Gaithersburg, MD, USA) according to the manufacturer's instructions.

Cell cycle analysis. The cells were fixed with 70% ethanol and stained with propidium iodide. The DNA content of the cells was evaluated using a FACS CantoII flow cytometer and FACS Diva software (BD, Franklin Lakes, NJ, USA).

Whole-exome sequencing. Targeted enrichment was performed using the SureSelect Human All Exon 50 Mb Kit (Agilent Technologies, Santa Clara, CA, USA) and sequenced using Illumina Genome Analyzer IIx (Illumina, San Diego, CA, USA).

Statistical analysis. Individual experiments were performed at least in triplicate. The statistical significance of observed differences was analyzed using Student's t-test. One asterisk (*) indicates a P-value smaller than 0.05. Two asterisks (**) indicate a P-value smaller than 0.01.

Results

Sensitivity of TE series cell lines to AZD2281. We tested the sensitivity of the TE series of ESCC cell lines to AZD2281 using clonogenic assays. All of the cell lines were cultured with various concentrations of AZD2281 for at least seven doubling times (10–16 days), and the number of colonies with more than 64 cells was counted. The concentrations of AZD2281 that caused a 50% reduction in clonogenic survival (IC_{50}) in the TE-6, TE-8, TE-10, TE-4, TE-11, TE-14, TE-9, and TE-1 cells were 0.4, 1.5, 2.2, 2.5, 3.0, 3.5, 5.5 and 6.5 μM, respectively (Figs 1a–c, S1). The IC_{50} values for HCC1937 and Capan-1 cells, which have deletions or mutations in the BRCA genes and are reported to be sensitive to PARP inhibitors,[22,23] were 0.2 and 0.6 μM, respectively. The IC_{50} values for MCF7 cells, which have wild-type BRCA genes and are known to be resistant to PARP inhibitors, was 8.0 μM. We further tested another PARP inhibitor, BSI-201. The IC_{50} values for TE-6 and TE-1 cells were 9.6 and 22.0 μM, respectively (Fig. S2). Because AZD2281 and BSI-201 suppressed the growth of the TE-6 cells as efficiently as it suppressed the growth of the BRCA-deficient, PARP-inhibitor-sensitive cell lines and failed to suppress the growth of the TE-1 cells; we designated TE-6 as a PARP inhibitor-sensitive ESCC cell line and TE-1 as a PARP inhibitor-resistant cell line. We selected these cells for further analyses.

AZD2281-induced G2/M arrest in TE-6 cells. To further study the mechanism of growth retardation of TE-6 cells by AZD2281, the status of the cell cycle in these cells was assessed by analyzing the DNA ploidy pattern (Figs 2a,b, S3). Treatment with 1 and 5 μM of AZD2281 for 12 h increased the population with 4n DNA content from 36.7% to 40.7% and 40.6%, respectively. Treatment for 24 h further increased the population with 4n DNA content from 31.6% to 37.9% and 46.3%, respectively. This suggested an increase in the G2 /M or M arrested population after AZD2281 treatment. On the other hand, no significant increase of tetraploid cells was observed in the TE-1 cells.

Increase of DSBs in TE-6 cells treated with AZD2281. To determine whether DSBs are formed after treatment with AZD2281 for 24 h, we assessed the amount of γ-H2AX as a marker of DSBs. Western blotting revealed that the level of γ-H2AX
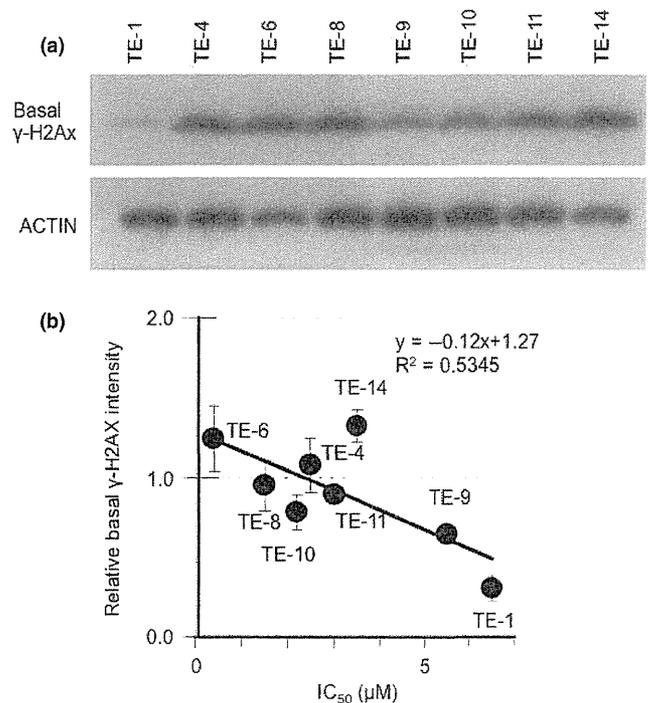
Fig. 4. A strong correlation between base-level γ-H2AX and sensitivity to AZD2281 of TE cells. (a) Eight non-treated TE-series cell lines were subjected to Western blot analysis with antibodies against γ-H2AX and actin. (b) The correlation between basal γ-H2AX expression levels and IC50 of AZD2281. The average intensity of γ-H2AX was standardized with actin. The data represent the averages and standard deviations of three independent experiments.

staining in TE-6 cells increased in a dose-dependent manner. However, no such increase was observed in TE-1 cells (Fig. 3a). The same trend was observed by immunofluorescence. Both the percentage of γ-H2AX positive cells determined by visual inspection and the average fluorescence intensity of γ-H2AX staining per cell increased significantly in a dose-dependent manner in TE-6 cells, but not in TE-1 cells, suggesting that AZD2281 induced an accumulation of DNA damage in TE-6 cells (Fig. 3b–d).

A strong correlation between base-level γ-H2AX and sensitivity to AZD2281 of TE cells. The Western blotting and immunofluorescence data also suggested that the baseline γ-H2AX level was higher in the AZD2281-sensitive TE-6 cells than in the resistant TE-1 cells (Fig. 3a). Because the increased amount of γ-H2AX may suggest the accumulation of DSBs, we evaluated the correlation between the basal expression levels of γ-H2AX and sensitivity to AZD2281 among the eight TE cell lines. A significant correlation between the basal levels of γ-H2AX and the IC_{50} of AZD2281 was observed ($R^2 = 0.5345$) (Fig. 4a,b).

Sustained X-ray irradiation-induced DSBs in TE-6 cells. To assess whether the impairment of DSB repair is relevant to the sensitivity of TE-series cells to AZD2281, we evaluated X-ray

Table 1. Tail moment of the X-ray-irradiated TE-6 and TE-1 cells

	Time after irradiation			
	0 h	15 min	2 h	6 h
TE-6	2.43 ± 3.19	5.27 ± 4.35	9.78 ± 6.27	13.7 ± 8.20
TE-1	3.69 ± 4.14	5.56 ± 3.97	5.20 ± 4.22	3.20 ± 4.71

(a)

(b)

(c)

(d)
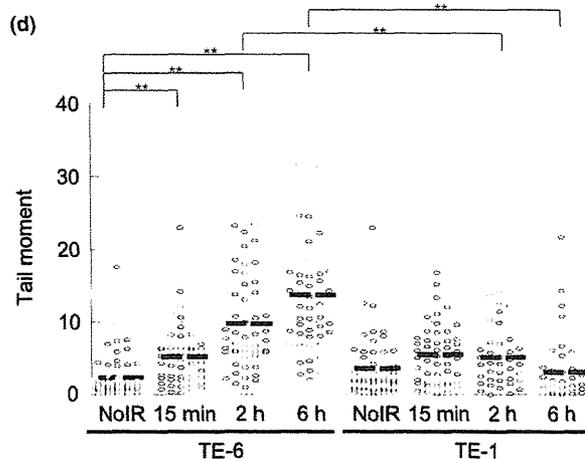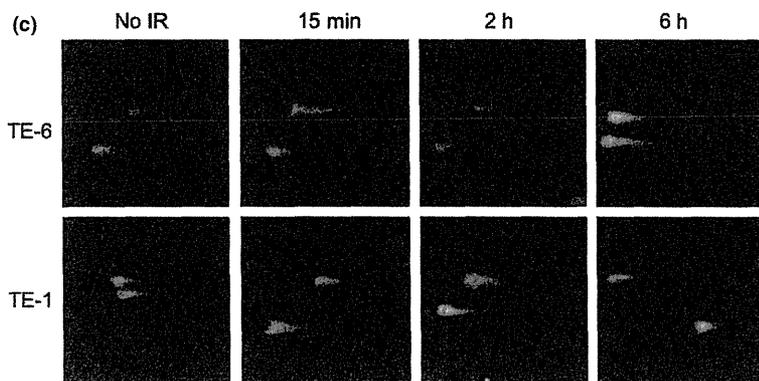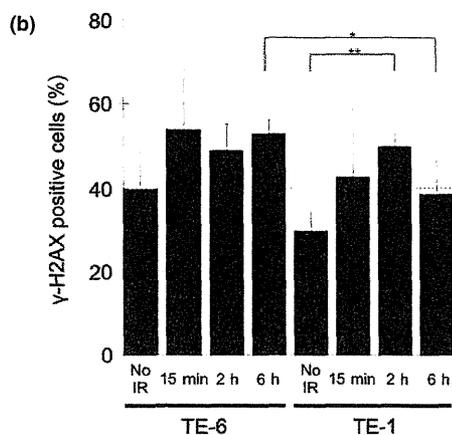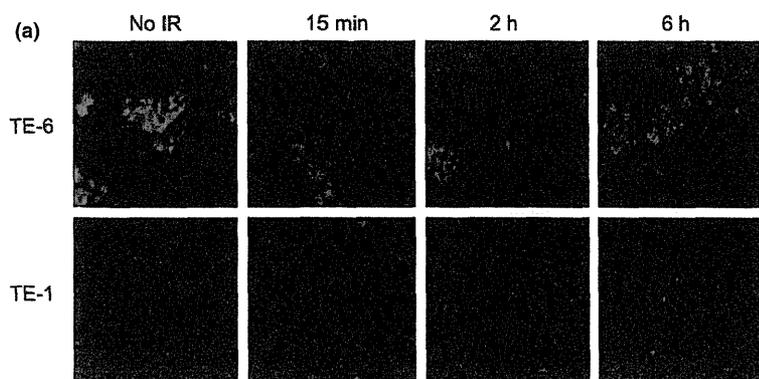
Fig. 5. Sustained X-ray irradiation-induced double strand breaks (DSBs) in TE-6 cells. (a) TE-6 and TE-1 cells were irradiated with 2 Gy X-ray. Cells were stained with anti-γ-H2AX antibody 15 min, 2 and 6 h after irradiation. (b) Percentages of γ-H2AX-positive cells. The data represent the average and standard deviations of three independent experiments. *P < 0.05, **P < 0.01 (Student's t-test). (c) Representative neutral comet assay results of TE-6 and TE-1 cells treated with or without 5 Gy of X-ray irradiation. (d) Scatter diagrams show the tail moment of individual TE-6 and TE-1 cells treated with or without 5 Gy of X-ray irradiation. The lines shown indicate the averages of the data plotted. The data were obtained from at least 100 cells for each condition. *P < 0.01 (Student's t-test).

Table 2. The number of nuclear foci of the DNA repair proteins

X-Ray (Gy)	53BP1			Rad51	
	0	2		0	10
Time	–	15 min	2 h	–	2 h
TE-6	0.55 ± 1.44	0.94 ± 1.12	1.48 ± 1.20	0.67 ± 2.20	2.25 ± 3.20
TE-1	1.09 ± 1.58	2.48 ± 2.44	4.86 ± 3.23	1.11 ± 1.50	3.65 ± 3.59

irradiation-induced DNA DSBs in these cells. First, the amount of γ-H2AX was assessed by immunfluorescence. As mentioned above, the γ-H2AX level of TE-6 cells was high at baseline and increased 15 min after irradiation and sustained for 6 h. In TE-1 cells, increase of γ-H2AX level was observed 2 h after irradiation, but declined after 6 h (Fig. 5a,b). Next, a neutral comet assay was performed to assess DNA damage. This assay detects a wide range of DNA lesions, including DSBs; the tail moment parameter is used as an index of DNA damage. We found a sustained increase in the tail moment of TE-6 cells (irradiation [–]; 2.43 ± 3.19, 15 min; 5.27 ± 4.35 2 h; 9.78 ± 6.27, 6 h; 13.71 ± 8.20), while in TE-1 cells, the tail moment transiently increased at 2 h after 5 Gy X-ray irradiation and then returned to the basal level at 6 h (irradiation [–]; 3.69 ± 4.14, 15 min; 5.56 ± 3.97 2 h; 5.20 ± 4.22, 6 h; 3.20 ± 4.71) (Fig. 5c,d, Table 1). These results suggested that the X-ray irradiation-induced DNA damage was properly repaired in the TE-1 cells but was sustained in the TE-6 cells.

Impairment of DSB repair protein nuclear foci formation in X-ray irradiated TE-6 cells. Because the TE-6 cells were found to be defective in DSB repair, we assessed the amount of BRCA1/2 expression in TE-series cells by Western blotting (Fig. S4a,b). However, no significant difference in the expression of BRCA1/2 in TE-6 and TE-1 cells was observed. To confirm the impairment of DNA repair machinery of TE-6 cells, we evaluated the nuclear focus formation of 53BP1, which is recruited to the γ-H2AX sites at an early stage in DSB repair, and RAD51, which is recruited at a late stage in DSB repair.[24–26] The baseline expression levels of 53BP1 and RAD51 were higher in the TE-6 cells (Fig. S5). However, increase of the number of 53BP1 nuclear foci per cell was much less in the TE-6 cells (irradiation [–]; 0.55 ± 1.44, 15 min; 0.94 ± 1.12 2 h; 1.48 ± 1.20), whereas 53BP1 foci were increased in the TE-1 cells (irradiation [–]; 1.09 ± 1.58, 15 min; 2.48 ± 2.44 2 h; 4.86 ± 3.23) (Fig. 6a,b, Table 2). Similarly, 6 h after 10 Gy X-ray irradiation, the number of RAD51 foci per cell was significantly increased in the TE-1 cells (irradiation [–]; 1.11 ± 1.50, 6 h; 3.65 ± 3.59), whereas the increase in RAD51 foci was not significant in the TE-6 cells (irradiation [–]; 0.67 ± 2.20, 2 h; 2.25 ± 3.20) (Fig. 6c,d, Table 2). These results suggested that the interaction between γ-H2AX and 53BP1 and the subsequent recruitment of RAD51 were impaired in TE-6 cells.

A novel mutation in the RNF8 gene, and the reduced ability of TE-6 cells to polyubiquitinate γ-H2AX. To identify the molecular mechanism underlying the impaired DNA repair in TE-6 cells, we performed whole-exome sequencing of TE-6 and TE-1 cells and selected the DNA repair-related genes that were mutated in the genomic DNA of TE-6 cells but not TE-1 cells. In total, 16 722 and 16 543 single nucleotide variants (SNV) were identified from the exomes of TE-1 and TE-6 cells, respectively (Tables S1 and S2). Another 260 and 240 indels were identified from TE-1 and TE-6 cells, respectively. To

reduce the probable germline variants, the single nucleotide polymorphisms (SNPs) that were registered in the dbSNP and in-house Japanese SNP databases were eliminated. Finaly, 606 SNVs and 118 indels were exclusively identified in the TE-6 cells. Among these mutations were hits in six genes (listed in Table 3) that are related to DNA repair. We further evaluated the impact of amino acid substitutions using the Polyphen2 prediction program; we focused in particular on the T448M missense mutation of RNF8, which is an E3-ligase polyubiquitylating γ-H2AX. The T448M mutation was close to the RING domain (Fig. 7a). To assess the ubiquitylation status of γ-H2AX, we examined X-ray-irradiated TE-6 and TE-1 cells by Western blotting (Fig. 7b). In the TE-1 cells, the levels of mono- and di-ubiquitinated γ-H2AX were increased at 2 h after irradiation and decreased at 6 h after irradiation. Meanwhile, no significant increase in ubiquitination was observed in the TE-6 cells (Fig. 7b–d).

Discussion

To date, the anti-tumor effects of PARP inhibitors to ESCC have not been evaluated both in vitro and in vivo. In this study, we identified TE-6 cells as AZD2281-sensitive cell line for the first time. The following findings support the idea that the PARP inhibitor induced growth retardation in the DSB repair-impaired background of TE-6 cells: (i) AZD2281 induced the accumulation of DNA damage, as evaluated by γ-H2AX expression levels. (ii) AZD2281 induced the accumulation of a tetraploid cell population in a time-dependent manner, consistent with previous reports that cells with accumulated unrepaired DSBs caused in every S-phase are arrested at G2/M boundary.[27] (iii) Sustained damage to DNA, the attenuated ubiquitination of γ-H2AX and a defect in DSB repair nuclear foci formation under X-ray irradiation suggest that TE-6 cells have an impaired DNA repair ability.

Several genomic biomarkers that predict the efficacy of PARP inhibitors have been identified. Though the presence or absence of BRCA1 and BRCA2 alterations most strikingly distinguishes the PARP inhibitor-sensitive cells and patients, no pathogenetic mutations in either gene were identified in the TE-6 cells (Table S1). Consistent with this, expression of BRCA1 and BRCA 2 proteins were not reduced in TE-6 cells (Fig. S3a,b). The alteration of other genes, such as 53BP1, RAD51, PTEN and USP11, also reportedly affects the sensitivity to PARP inhibitors.[18,28–32] To identify the genomic events corresponding to the AZD2281 sensitivity of TE-6 cells, we performed whole-exome sequencing. Because a paired non-tumor genome is not available for the TE-series cells, we subtracted previously identified germline variants from our set of total SNVs and indels to enrich for potential somatic mutations. Among the remaining mutations, we focused on those located in the genes encoding DNA repair-related proteins and identified a novel mutation of RNF8. RNF8 is an E3-ligase

Original Article
PARP inhibitor-sensitive ESCC cells
www.wileyonlinelibrary.com/journal/cas
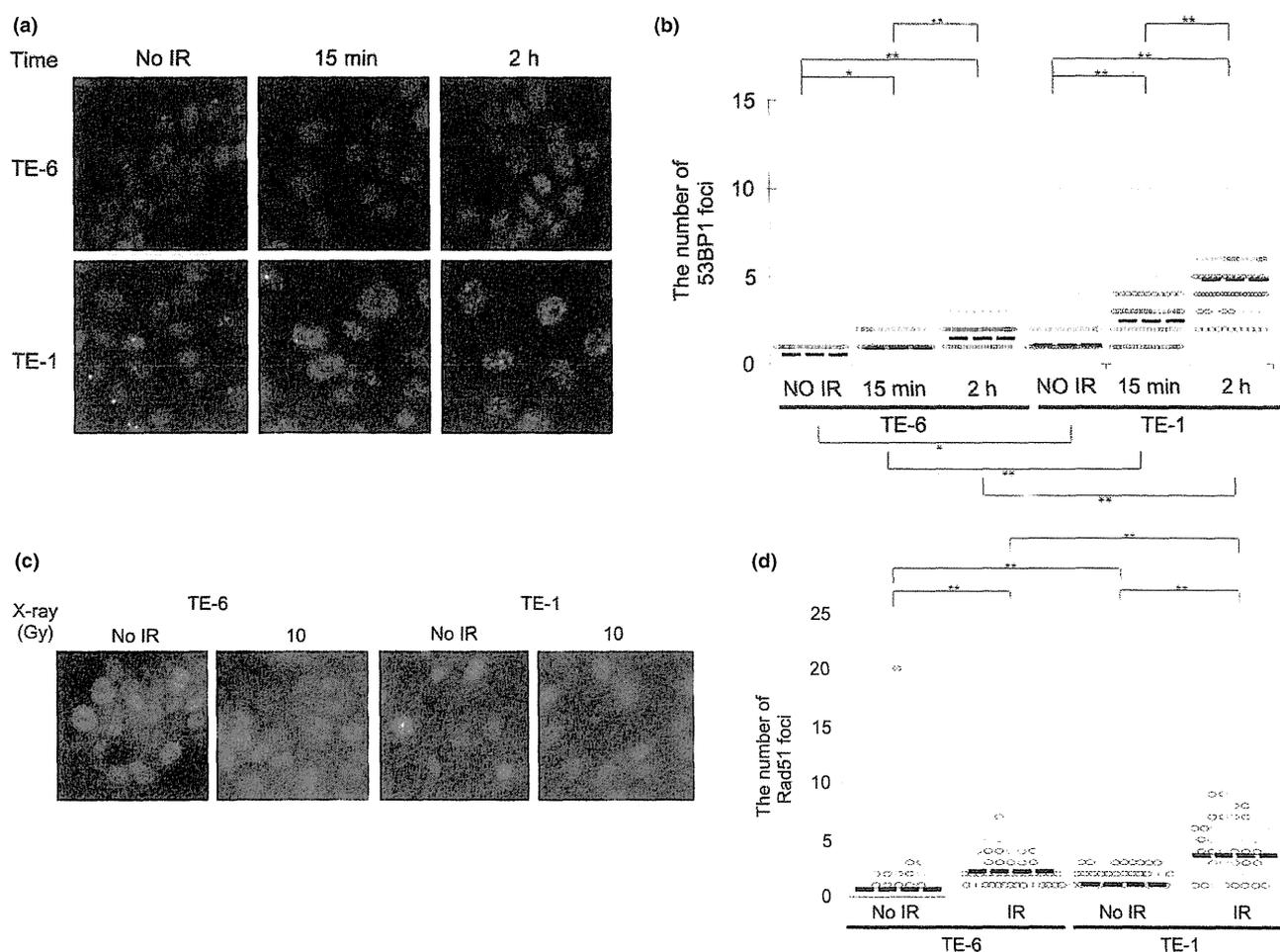
Fig. 6. Impairment of 53BP1 and RAD51 nuclear focus formation in X-ray irradiated TE-6 cells. (a) TE-6 and TE-1 cells were irradiated with 2 Gy of X-rays and fixed 15 min and 2 h after irradiation. The formation of 53BP1 nuclear foci was evaluated by immunofluorescence. (b) Scatter diagrams showing the number of 53BP1 foci in individual cells. The lines shown indicate the mean of the data plotted. The data were obtained from at least 100 cells for each condition. $*P < 0.05$, $**P < 0.01$ (Student's t-test). (c) TE-6 and TE-1 cells were irradiated with 10 Gy of X-rays and fixed 6 h after irradiation. The formation of RAD51 nuclear foci was evaluated by immunofluorescence. (d) Scatter diagrams showing the number of RAD51 foci in individual cells. The lines shown indicate the mean of the data plotted. The data were obtained from at least 100 cells for each condition. $**P < 0.01$ (Student's t-test).

Table 3. Mutations in the DNA repair-related genes uniquely identified in the exome of TE-6 cells

Novel mutations of DNA repair involved genes of TE-6

Gene	Chr.	Position	Base change	Variant frequency (%)	Amino acid alteration	PolyPhen2 prediction
RNF8	6	37349032	C>T	100	T448M	Probably damaging
CHAF1A	19	4429530	G>A	87	R567Q	Probably damaging
CEP164	11	117222670	A>G	88.9	D120G	Probably damaging
CLSPN	1	36217027	C>T	19.4	A618T	Benign
POLK	5	74865291	A>G	55	I128V	Benign
ATRX	X	76952184	G>A	100	S84L	Benign

targeting γ-H2AX that accumulates at DNA DSBs and recruits repair proteins, including 53BP1 and RAD51.[33–35] It was reported that $RNF8^{-/-}$ $p53^{-/-}$ mice had increased levels of

genomic instability and a remarkably elevated tumor incidence compared to $p53^{-/-}$ mice,[36] that the knockdown of RNF8 sensitized cells to ionizing radiation, and that disruption of the RING domains of RNF8 impaired DSB-associated ubiquitylation and inhibited retention of 53BP1 and BRCA1 at the DSBs sites.[33] The PolyPhen-2 program predicts a probable deleterious impact of the T448M substitution on the structure and function of RNF8. Although the effect of the T448M mutation on the polyubiquitination ability of RNF8 has not yet been confirmed, the observation that the increase in ubiquitination after X-ray irradiation in the TE-6 cells was less than that of the TE-1 cells suggests that RNF8 is impaired in the TE-6 cells. We hypothesized that this mutation might affect the polyubiquitination ability of RNF8 and, as a result, contribute to the DSB repair defect to some extent. The impact of the mutation or loss of RNF8 to PARP inhibitor sensitivity has to be further evaluated.

Whether RNF8 is the only factor contributing to TE-6 sensitivity should be carefully considered. The anti-tumor effect of PARP inhibitors is obviously determined by the BRCA1 or BRCA2 status in ovarian and breast cancers.[37] Meanwhile, the sensitivity of the TE-series cells to AZD2281 is altered by
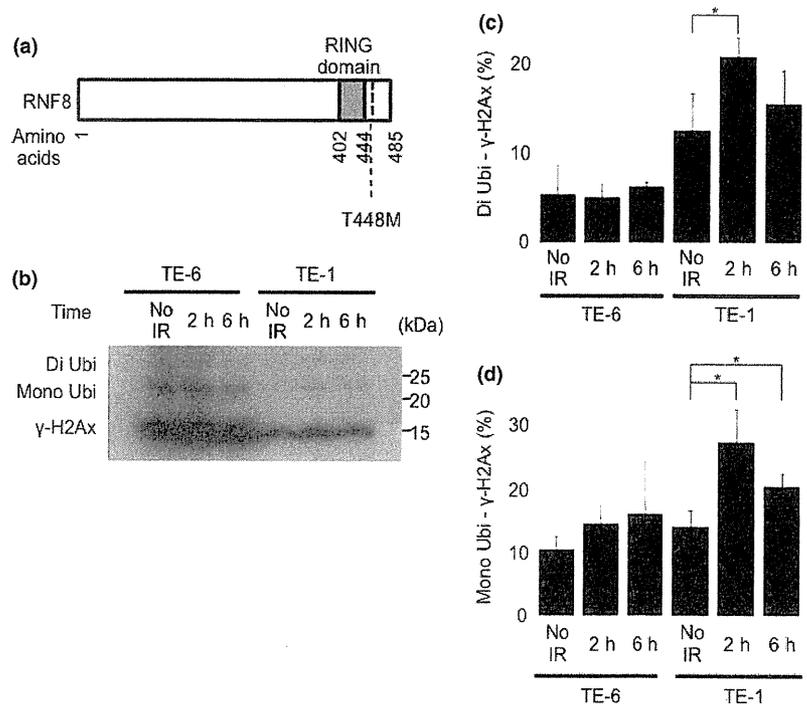
Fig. 7. A novel mutation in the RNF8 gene and the reduced ability of TE-6 cells to polyubiquitinate γ-H2AX. (a) The structure of RNF8 protein and a newly identified T448M amino acid-substitution mutation. (b) Western blot analysis of γ-H2Ax in TE-6 and TE-1 cells treated with 2 Gy of X-rays. (c) The proportion of diubiquitinated γ-H2Ax standardized to non-ubiquitinated γ-H2Ax. The data represent the averages and standard deviations of three independent experiments. (d) The proportion of monoubiquitinated γ-H2Ax standardized to non-ubiquitinated γ-H2Ax. The data represent the averages and standard deviations of three independent experiments.

gradation and most cells exhibited intermediate sensitivity. It may suggest that the AZD2281 sensitivity was regulated by multiple molecular mechanisms in each cell line rather than a single molecule. This multiplicity might make it difficult to identify the distinctive genomic biomarkers of PARP inhibitor sensitivity in ESCC.

We noticed a strong correlation between AZD2281 sensitivity and γ-H2Ax levels in the cells without treatment; this effect might represent the extent of baseline DNA damage. Double strand breaks regularly occur in proliferating cells because topoisomerases bind to DNA and cut the phosphate backbone of the DNA during DNA replication. Though these DSBs are properly repaired in non-tumor cells, it is plausible that unrepaired DNA remains in tumor cells with impaired DSB repair, such as the TE-6 cells. Once a correlation between the baseline level of γ-H2Ax expression and DSB

repair defect is further confirmed, the amount of γ-H2Ax in a tumor tissue sample could be a reasonable biomarker for selecting preferable patients for PARP inhibitor therapy. Further clinical and biological studies of this effect are warranted.

Acknowledgments

Disclosure Statement

The authors have no conflict of interest.

References

1 Jemal A, Bray F, Center MM, Ferlay J, Ward E, Forman D. Global cancer statistics. *CA Cancer J Clin* 2011; **61**: 69–90.

2 Jamieson GG, Mathew G, Ludemann R, Wayman J, Myers JC, Devitt PG. Postoperative mortality following oesophagectomy and problems in reporting its rate. *Br J Surg* 2004; **91**: 943–7.

3 Müller JM, Erasmi H, Stelzner M, Zieren U, Pichlmaier H. Surgical therapy of oesophageal carcinoma. *Br J Surg* 1990; **77**: 845–57.

4 Zhang X, Watson DI, Jamieson GG, Lally C, Bessell JR, Devitt PG. Outcome of oesophagectomy for adenocarcinoma of the oesophagus and oesophagogastric junction. *ANZ J Surg* 2005; **75**: 513–9.

5 Crumley AB, Going JJ, McEwan K *et al.* Endoscopic mucosal resection for gastroesophageal cancer in a U.K. population. Long-term follow-up of a consecutive series. *Surg Endosc* 2011; **25**: 543–8.

6 Lewis JJ, Rubenstein JH, Singal AG, Elmunzer BJ, Kwon RS, Piraka CR. Factors associated with esophageal stricture formation after endoscopic mucosal resection for neoplastic Barrett's esophagus. *Gastrointest Endosc* 2011; **74**: 753–60.

7 Fujishiro M, Yahagi N, Kakushima N *et al.* Endoscopic submucosal dissection of esophageal squamous cell neoplasms. *Clin Gastroenterol Hepatol* 2006; **4**: 688–94.

8 Herskovic A, Martz K, al-Sarraf M *et al.* Combined chemotherapy and radiotherapy compared with radiotherapy alone in patients with cancer of the esophagus. *N Engl J Med* 1992; **326**: 1593–8.

9 al-Sarraf M, Martz K, Herskovic A *et al.* Progress report of combined chemoradiotherapy versus radiotherapy alone in patients with esophageal cancer: an intergroup study. *J Clin Oncol* 1997; **15**: 277–84.

10 Ame JC, Spenlehauer C, de Murcia G. The PARP superfamily. *BioEssays* 2004; **26**: 882–93.

11 Gallmeier E, Kern SE. Absence of specific cell killing of the BRCA2-deficient human cancer cell line CAPAN1 by poly(ADP-ribose) polymerase inhibition. *Cancer Biol Ther* 2005; **4**: 703–6.

12 Bryant HE, Schultz N, Thomas HD *et al.* Specific killing of BRCA2-deficient tumours with inhibitors of poly(ADP-ribose) polymerase. *Nature* 2005; **434**: 913–7.

13 Venkitaraman AR. Cancer susceptibility and the functions of BRCA1 and BRCA2. *Cell* 2002; **108**: 171–82.

14 Weston VJ, Oldreive CE, Skowronska A *et al.* The PARP inhibitor olaparib induces significant killing of ATM-deficient lymphoid tumor cells in vitro and in vivo. *Blood* 2010; **116**: 4578–87.

15 Williamson CT, Muzik H, Turhan AG *et al.* ATM deficiency sensitizes mantle cell lymphoma cells to poly(ADP-ribose) polymerase-1 inhibitors. *Mol Cancer Ther* 2010; **9**: 347–57.

16 Dedes KJ, Wetterskog D, Mendes-Pereira AM *et al.* PTEN deficiency in endometrioid endometrial adenocarcinomas predicts sensitivity to PARP inhibitors. *Sci Transl Med* 2010; **2**: 53–75.

17 McEllin B, Camacho CV, Mukherjee B *et al.* PTEN loss compromises homologous recombination repair in astrocytes: implications for glioblastoma therapy with temozolomide or poly(ADP-ribose) polymerase inhibitors. *Cancer Res* 2010; **70**: 5457–64.

18 Wiltshire TD, Lovejoy CA, Wang T, Xia F, O'Connor MJ, Cortez D. Sensitivity to poly(ADP-ribose) polymerase (PARP) inhibition identifies ubiquitin-specific peptidase 11 (USP11) as a regulator of DNA double-strand break repair. *J Biol Chem* 2010; **285**: 14565–71.

19 Akbari MR, Malekzadeh R, Lepage P *et al.* Mutations in Fanconi anemia genes and the risk of esophageal cancer. *Hum Genet* 2011; **129**: 573–82.

20 Rosenberg PS, Alter BP, Ebell W. Cancer risks in Fanconi anemia: findings from the German Fanconi Anemia Registry. *Haematologica* 2008; **93**: 511–7.

21 Stransky N, Egloff AM, Tward AD *et al.* The mutational landscape of head and neck squamous cell carcinoma. *Science* 2011; **333**: 1157–60.

22 Drew Y, Mulligan EA, Vong WT *et al.* Therapeutic potential of poly(ADP-ribose) polymerase inhibitor AG014699 in human cancers with mutated or methylated BRCA1 or BRCA2. *J Natl Cancer Inst* 2011; **103**: 334–46.

23 Sakai W, Swisher EM, Karlan BY *et al.* Secondary mutations as a mechanism of cisplatin resistance in BRCA2-mutated cancers. *Nature* 2008; **451**: 1116–20.

24 Rodrigue A, Lafrance M, Gauthier MC *et al.* Interplay between human DNA repair proteins at a unique double-strand break in vivo. *EMBO J* 2006; **25**: 222–31.

25 Mochan TA, Venere M, DiTullio RA Jr, Halazonetis TD. 53BP1, an activator of ATM in response to DNA damage. *DNA Repair (Amst)* 2004; **3**: 945–52.

26 Baumann P, West SC. Role of the human RAD51 protein in homologous recombination and double-stranded-break repair. *Trends Biochem Sci* 1998; **23**: 247–51.

27 Farmer H, McCabe N, Lord CJ *et al.* Targeting the DNA repair defect in BRCA mutant cells as a therapeutic strategy. *Nature* 2005; **434**: 917–21.

28 Bunting SF, Callén E, Wong N *et al.* 53BP1 inhibits homologous recombination in Brca1-deficient cells by blocking resection of DNA breaks. *Cell* 2010; **141**: 243–54.

29 McCabe N, Turner NC, Lord CJ *et al.* Deficiency in the repair of DNA damage by homologous recombination and sensitivity to poly(ADP-ribose) polymerase inhibition. *Cancer Res* 2006; **66**: 8109–15.

30 Mendes-Pereira AM, Martin SA, Brough R *et al.* Synthetic lethal targeting of PTEN mutant cells with PARP inhibitors. *EMBO Mol Med* 2009; **1**: 315–22.

31 Turner NC, Ashworth A. Biomarkers of PARP inhibitor sensitivity. *Breast Cancer Res Treat* 2011; **127**: 283–6.

32 Wang X, Weaver DT. The ups and downs of DNA repair biomarkers for PARP inhibitor therapies. *Am J Cancer Res* 2011; **1**: 301–27.

33 Mailand N, Bekker-Jensen S, Faustrup H *et al.* RNF8 ubiquitylates histones at DNA double-strand breaks and promotes assembly of repair proteins. *Cell* 2007; **131**: 887–900.

34 Bekker-Jensen S, Mailand N. Assembly and function of DNA double-strand break repair foci in mammalian cells. *DNA Repair (Amst)* 2010; **9**: 1219–28.

35 Lu CS, Truong LN, Aslanian A *et al.* The RING finger protein RNF8 ubiquitinates Nbs1 to promote DNA double-strand break repair by homologous recombination. *J Biol Chem* 2012; **287**: 43984–94.

36 Halaby MJ, Hakem A, Li L *et al.* Synergistic interaction of Rnf8 and p53 in the protection against genomic instability and tumorigenesis. *PLoS Genet* 2013; **9**: e1003259.

37 Fong PC, Boss DS, Yap TA *et al.* Inhibition of poly(ADP-ribose) polymerase in tumors from BRCA mutation carriers. *N Engl J Med* 2009; **361**: 123–34.

Supporting Information

Additional supporting information may be found in the online version of this article:

Data S1. Materials and methods.

Fig. S1. Effect of AZD2281 on the colony formation of TE-8, TE-10, TE-4, TE-11, TE-14, TE-9 and HCC1937 cells.

Fig. S2. Effect of BSI-201 on the colony formation of TE-1 and TE-6 cells.

Fig. S3. DNA ploidy of TE-1 andTE-6 cells treated with AZD2281 for 12 h.

Fig. S4. Expression of the BRCA1 and BRCA2 proteins in TE-series cells.

Fig. S5. Expression of the 53BP1 and RAD51 proteins in TE-1 and TE-6 cells.

Table S1. Summary of the whole exome sequencing data of TE-1 cells.

Table S2. Summary of the whole exome sequencing data of TE-6 cells.

Identification and Characterization of Cancer Mutations in Japanese Lung Adenocarcinoma without Sequencing of Normal Tissue Counterparts

Ayako Suzuki[1©], Sachiyo Mimaki[2©], Yuki Yamane[3], Akikazu Kawase[3], Koutatsu Matsushima[2], Makito Suzuki[2], Koichi Goto[3], Sumio Sugano[1], Hiroyasu Esumi[2], Yutaka Suzuki[1*], Katsuya Tsuchihara[2]

1 Department of Medical Genome Sciences, Graduate School of Frontier Sciences, The University of Tokyo, Chiba, Japan, 2 Division of Translational Research, Research Center for Innovative Oncology, National Cancer Center Hospital East, Chiba, Japan, 3 Thoracic Oncology Division, National Cancer Center Hospital East, Chiba, Japan

Abstract

We analyzed whole-exome sequencing data from 97 Japanese lung adenocarcinoma patients and identified several putative cancer-related genes and pathways. Particularly, we observed that cancer-related mutation patterns were significantly different between different ethnic groups. As previously reported, mutations in the EGFR gene were characteristic to Japanese, while those in the KRAS gene were more frequent in Caucasians. Furthermore, during the course of this analysis, we found that cancer-specific somatic mutations can be detected without sequencing normal tissue counterparts. 64% of the germline variants could be excluded using a total of 217 external Japanese exome datasets. We also show that a similar approach may be used for other three ethnic groups, although the discriminative power depends on the ethnic group. We demonstrate that the ATM gene and the PAPPA2 gene could be identified as cancer prognosis related genes. By bypassing the sequencing of normal tissue counterparts, this approach provides a useful means of not only reducing the time and cost of sequencing but also analyzing archive samples, for which normal tissue counterparts are not available.

Introduction

The advent of next generation sequencing technology has greatly facilitated the detection and characterization of genetic variations in the human genome. Most remarkably, this type of study has driven the 1000 Genomes Project [1,2], which aims to provide a comprehensive map of human genetic variants across various ethnic backgrounds. However, because whole-genome sequencing is still costly, the sequencing of whole exon regions using hybridization capture methods (exome sequencing) [3-5] is widely used to screen for genes that are related to hereditary diseases. By sequencing exomes from healthy and diseased individuals and comparing them, genes that are responsible for many diseases have been identified [6], including Miller syndrome [7,8] and familial hyperkalemic hypertension [9]. Along with the progress that has been made in exome sequencing, the volume of germline single nucleotide

polymorphism (SNP) data that has been registered in dbSNP is rapidly expanding for various populations [10].

Exome sequencing provides a powerful tool for cancer studies as well. Indeed, a number of papers have been published describing the identification and characterization of single nucleotide variants (SNVs) that somatically occur in cancers and are suspected to be responsible for carcinogenesis and disease development [11]. The International Cancer Genome Consortium (ICGC) has been collecting exome data for somatic SNVs that are present in more than 50 types of cancers as a part of an international collaborative effort [12-14]. The Cancer Genome Atlas (TCGA) has developed a large genomic dataset, including exomes for high-grade ovarian carcinoma, that has been used to detect significantly mutated genes, including TP53, BRCA1 and BRCA2 [15]. They have also identified various genomic aberrations and deregulated pathways that may act as therapeutic targets.

In most ongoing cancer exome studies, normal tissue counterparts have been sequenced in parallel with cancer tissue [15-19]. This is assumed to be necessary because germline variants must be excluded from the full set of SNVs to detect the somatic SNVs that are unique to cancers. However, the sequencing of normal tissue counterparts increases the cost and time of the analysis. Also, in some cases, it is difficult to obtain normal tissue counterparts. In addition, it remains unclear how accurately germline SNVs can be excluded using normal tissue exomes. To conservatively exclude germline SNVs, their sequence depths and accuracies may need to be greater than those that are obtained from the cancer exomes.

In this study, we generated and analyzed 97 cancer exomes from Japanese lung adenocarcinoma patients. We also demonstrate that somatic SNVs can be enriched to a level that is sufficient for further statistical analyses even in the absence of the sequencing of normal tissue counterparts. To separate the germline from the somatic SNVs, we first compared the variation patterns between a cancer exome with the 96 other patients' normal tissue exomes. We also attempted to conduct a similar mutual comparison solely utilizing cancer exomes, without the consideration of exomes of normal tissue counterparts. It is true that if we completely omitted normal tissue sequencing, we would tentatively disregard of somatic mutations that occurs at exactly the same genomic position in multiple cancers. However, recent papers have elucidated that such shared SNVs are very rare [15,20-22]. Moreover, many of these recursively mutations have been registered in the cancer somatic mutation databases such as Sanger COSMIC [23,24], and those recurrent SNVs can be recovered by follow-up studies partially using the data from the normal tissues. To understand the unique nature of each cancer, a statistical analysis of the distinct SNVs is presumed to be essential in addition to the analysis of the common SNVs.

In this study, we demonstrate that it is possible to identify the first candidates for cancer-related genes and pathways, even without the sequencing of a normal tissue counterpart. We show that this approach is useful not only to reduce the cost of the sequencing but also to improve the fidelity of the data. It should be also useful for analyzing old archive samples, for which normal tissue counterparts are not always available. Here, we describe a practical and cost-effective method to expedite cancer exome sequencing.

Results and Discussion

Characterization of SNVs using the 97 exome dataset

Firstly, we generated and analyzed whole-exome sequences from 97 Japanese lung adenocarcinoma patients. Exome data were collected from both cancer and normal-tissue counterparts, separated by laser capture microdissection. We purified the exonic DNA (exomes) and generated 76-base paired-end reads using the illumina GAIIx platform. Approximately 30 million mapped sequences were obtained from each sample, providing 74× coverage of the target regions; 93% of the target regions had 5× coverage (Figure S1 in File S1). Burrows-Wheeler Aligner (BWA) [25] and the Genome Analysis Toolkit (GATK) [26,27] were used to identify

SNVs (Figure S2 in File S1). Only SNVs that were detected in cancer tissues and showed no evidence of variation in normal tissues were selected for further analysis.

The obtained dataset was used to characterize the cancer-specific mutation patterns (Table S3 in File S1). We calculated the enrichment of the SNVs within particular genes, protein domains, functional categories, and pathways. We searched for genes with somatic SNVs significantly enriched in Japanese lung adenocarcinoma. As shown in Table S4 in File S1, several genes were identified as significantly mutated. In particular, we searched for domains that are enriched with SNVs and harbor known cancer-related mutations in the COSMIC database. In total, 11 genes were identified (P < 0.02, Table 1). For example, the Dbl homology (DH) domain of PREX1 gene [28] was enriched with SNVs (P = 0.00071). However, in the PREX2 gene [29], the Pleckstrin homology (PH) domain was enriched with SNVs (P = 0.011) (Figure 1A and B). Both the PREX1 and the PREX2 genes activate the exchange of GDP to GTP for the Rho family of GTPases and the DH/PH domains are indispensable for nucleotide exchange of GTPases and its regulation [30-32]. In addition, we analyzed the expression patterns of these genes using a cancer gene expression database, GeneLogic (Figure S3 in File S1). Expression levels of PREX1 and PREX2 were not enhanced in lung adenocarcinoma but were enhanced in wide variety of cancers, which is partly indicated in previous studies [33]. The SNVs in the PREX1 and PREX2 genes, which were concentrated at its pivotal signaling domains, might enhance activities in these genes, and thereby functionally mimics the increased expressions of this gene in some different types of cancers. The cancer-related gene candidates identified from this dataset are listed in Table 1.

Similarly, pathway enrichment analyses using the KEGG database [34] also detected several putative cancer-related pathways. The identified pathways are listed in Table 2. Interestingly, the endometrial cancer pathway [35] was detected in this enrichment analysis (P = 3.1e-15, Figure 2A). This pathway includes major cancer-related pathways, for example, the MAPK signaling pathway and the PI3K/AKT pathway. For this pathway, we compared mutation patterns between our Japanese data and those of the previous study of lung adenocarcinoma in Caucasians [21]. We found that the SNVs in the EGFR gene were four times more frequent in the Japanese population than among Caucasian populations (Figure 2B, left panel). EGFR mutations were frequently occurring in non-smoker, female and Asian patients of lung adenocarcinoma [36], which is a molecular target of anti-cancer drug, gefitinib [20,37,38]. Conversely, KRAS mutations, which are also well-known cancer-related mutations [39], were more than four times frequent among Caucasians (Figure 2B, center panel). However not all mutational patterns are different between populations. For instance, TP53 harbored mutations in both datasets with similar frequency (Figure 2B, right panel).

Ambiguity in SNV identification of normal tissue counterparts

In the aforementioned analysis, we discriminated germline variants using the normal tissue counterparts. A number of

Table 1. List of the identified possible cancer-related genes.

Gene	Domain	Number of SNVs Domain	Gene	P-value*
EGFR†	IPR001245:Serine-threonine/tyrosine-protein kinase	34	37	4.4e-21
KRAS†	IPR001806:Ras GTPase	6	7	8.0e-6
TNN	IPR003961:Fibronectin, type III	4	5	5.2e-5
TP53†	IPR008967:p53-like transcription factor, DNA-binding	20	23	9.5e-5
PREX1	IPR000219:Dbl homology (DH) domain	4	5	0.00071
DNAH7	IPR004273:Dynein heavy chain	5	7	0.0025
FSTL5	IPR011044:Quinoprotein amine dehydrogenase, beta chain-like	7	7	0.0043
NRXN3	IPR008985:Concanavalin A-like lectin/glucanase	5	7	0.0063
PREX2	IPR001849:Pleckstrin homology	3	7	0.011
FER1L6	IPR008973:C2 calcium/lipid-binding domain, CaLB	3	6	0.013
COL22A	IPR008985:Concanavalin A-like lectin/glucanase	3	6	0.015

*P < 0.02

† Reported in the Cancer Gene Census [11]. Note that the genes atop the list are previously reported to be associated with this cancer type, while most of them are novel possible cancer-related genes.

doi: 10.1371/journal.pone.0073484.t001

SNVs initially identified as somatic were also found to be present in normal tissues, thus, were false positive calls under the validations by visual inspection of the mapped sequences and Sanger sequencing. To examine the cause of this problem, we inspected the errors in randomly selected 26 cancers and their normal tissues. On average in each cancer, twenty-five percent of somatic SNV candidates were found to be false positive (Figure 3). In these cases, the sequence coverage and quality of the normal counterpart were not sufficient. Indeed, the sequences supporting each SNV and these qualities were significantly diverged between the cancer and normal tissues. Although we increased the total number of reads in the normal tissues, it was difficult in practice to cover all of the genomic positions (Figure S4 in File S1). A summary of the germline SNV validations is shown in Table S5 in File S1.

However, we noticed that some were correctly identified as germline SNVs in external reference exomes. Twenty-five exomes allowed us to exclude eight false positive calls in each cancer. This raised the possibility that the SNVs from the other patients may be used as surrogates to increase the depth and quality of the sequencing.

Excluding germline SNVs by considering mutual overlaps of other persons' exomes

To further test this possibility, we examined whether cancer exome analyses would be possible without sequencing of the normal tissue counterpart of each cancer. First, we evaluated the extent to which the germline SNVs could be discriminated using external exomes. For this purpose, we used the 97

paired cancer-normal exome datasets for the validation dataset. We found that we could detect 54% of the germline SNVs by using the 96 normal tissue exomes from the external reference (Figure 4A). We further expanded the filtration dataset using the externally available 73 Japanese exome data and 48 in-house Japanese exome datasets. Altogether, we were able to remove 64% of the germline SNVs, using a total of 217 Japanese exome datasets from other individuals, without sequencing each cancer's normal counterpart (Figure 4A). The extrapolation of the graph also indicated that 1,350 and 2,000 samples would be required to remove 90% and 95% of the germline SNVs, respectively. We expect that such a sample size will be available in near future considering current rapid expansion of the exome analysis.

We further evaluated if the same filtration could be done by solely using cancer exomes. We obtained essentially the same results (Figure S5 in File S1). Obvious caveat of this approach is that this would disregard about 3% of somatic SNVs recurrently occurring (Figure S5 in File S1, blue). However, as aforementioned, we found that those recurrent SNVs were very rare [15,19] and most of them were derived from dubious somatic SNVs, which were overlooked in the normal tissues. We also consider that most of those recurrent SNVs, if any, can be analyzed separately by sequencing a limited number of normal tissues.

Filtering out germline SNVs by considering mutual overlaps for different ethnic groups and for rare SNPs

We examined whether SNVs in other ethnic backgrounds could be used as external datasets for the filtration. We obtained exome data from individuals of various ethnic backgrounds from the 1000 Genome Project. We used these exome datasets to exclude the germline SNVs that were identified in the Japanese cancers. We found that the discriminative power was significantly lower compared with exomes from Japanese populations. Therefore, these datasets were not suitable for this purpose (Figure 4B). We also examined and found that the exomes in each ethnic group were useful to discriminate the germline SNVs in the corresponding group (Figure S6, S7 and Table S6 in File S1).

We, then, examined to what extent minor germline variants could be covered with this approach in the Japanese population. We evaluated the sensitivity of the filtration process for the SNVs in the 97 cancers (Figure S8 in File S1). We found that 88% of the germline SNVs occurring in more than five percent of the 97 exomes could be detected using the 73 external Japanese datasets. For the SNVs occurring in 1% of the 97 cancers, 19% could be excluded.

Using the crude dataset to characterize cancer related SNVs and pathways

Taken together, with 217 Japanese exomes used for filtration, 36% of the germline SNVs remained unfiltered. Nevertheless, we considered that it may be still possible to use the crude SNV dataset as a first approximation for identifying and analyzing cancer-related genes and pathway candidates. To validate this idea, we compared the results of enrichment analyses between the crude dataset and the refined somatic
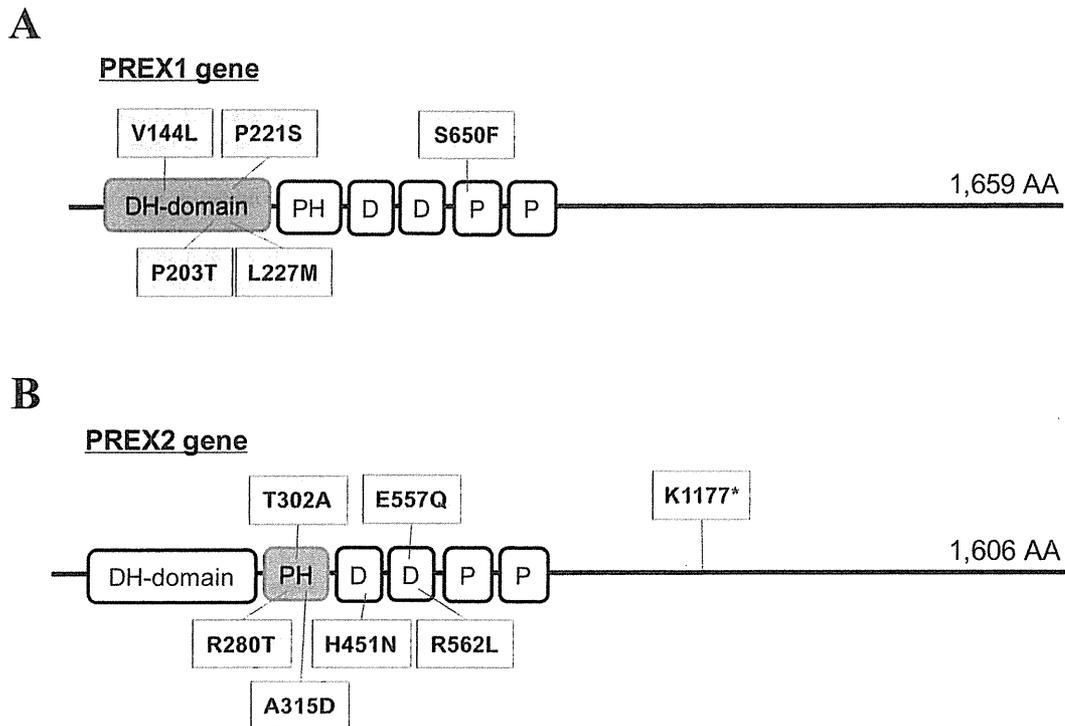
A

PREX1 gene

B

PREX2 gene

Figure 1. Identification and characterization of the putative cancer-related genes using 97 cancer exomes. SNVs in the PREX1 (A) and PREX2 (B) genes are represented in the boxes. The protein domains in which the enrichments of the SNVs were statistically significant are represented in orange boxes (also see Materials and Method). DH-domain: Dbl homology (DH) domain; PH: Pleckstrin homology domain; D: DEP domain; P: PDZ/DHR/GLGF.

doi: 10.1371/journal.pone.0073484.g001

SNV datasets, which were generated from the paired cancer-normal exomes.

Most of the putative cancer-related genes and pathways that were identified from the refined dataset were also present in the crude dataset (Tables S7 and S8 in File S1). The example of the TNN gene, which was reported as a marker of tumor stroma [40–42], is shown in Figure S9 in File S1. In this case, even with the germline SNVs, which were unfiltered in the crude dataset (indicated by black in Figure S9 in File S1), the enrichment of somatic SNVs in this domain was statistically significant. In total, nine genes which identified as possessing cancer-related SNVs from the refined dataset were also detected in the crude dataset. On the other hand, two genes from the refined dataset were not represented in the crude dataset. In the pathway analysis, we identified 26 cancer-related pathways which were identified from the refined

dataset. In addition, 19 pathways were also represented in the crude dataset as well as the refined dataset. The overlap between the datasets is summarized in Table 3. It should be noted that statistically enrichment analyses were possible even at the current coverage of the filter dataset. With the expanded external dataset, it would be more practical to subject the candidates to the results of Sanger sequencing validations as well as removing remaining germline SNVs.

Identification of prognosis related genes by using the crude dataset

As one of the most important objectives of the cancer exome studies, we investigated whether mutations affecting cancer prognoses can be identified by using crude dataset (Table S9 and Figure S10 in File S1). In the Kaplan-Meier analysis, seven patients who carried SNVs in the ATM gene (Figure 5A)

Table 2. List of the identified possible cancer-related pathways.

KEGG ID	Pathway definition	Number of cancers with SNVs	P-value*
hsa05213	Endometrial cancer	72	3.1e-15
hsa04320	Dorso-ventral axis formation	48	4.4e-15
hsa05219	Bladder cancer	62	4.9e-14
hsa05223	Non-small cell lung cancer	66	7.1e-12
hsa05214	Glioma	70	6.5e-11
hsa05218	Melanoma	70	1.3e-9
hsa05212	Pancreatic cancer	68	6.9e-9
hsa05215	Prostate cancer	71	4.3e-7
hsa05216	Thyroid cancer	36	1.1e-6
hsa04520	Adherens junction	59	3.7e-6
hsa05210	Colorectal cancer	53	1.8e-5
hsa04012	ErbB signaling pathway	64	2.6e-5
hsa05120	Epithelial cell signaling in *Helicobacter pylori* infection	53	4.8e-5
hsa04540	Gap junction	60	0.00024
hsa04912	GnRH signaling pathway	61	0.0011
hsa05217	Basal cell carcinoma	41	0.0020
hsa05222	Small cell lung cancer	52	0.0069
hsa05220	Chronic myeloid leukemia	46	0.010
hsa05160	Hepatitis C	67	0.012
hsa05014	Amyotrophic lateral sclerosis (ALS)	36	0.014
hsa04977	Vitamin digestion and absorption	20	0.015
hsa05416	Viral myocarditis	40	0.028
hsa04512	ECM-receptor interaction	47	0.034
hsa02010	ABC transporters	29	0.035
hsa04510	Focal adhesion	78	0.037
hsa05412	Arrhythmogenic right ventricular cardiomyopathy (ARVC)	40	0.039

*$P < 0.05$

doi: 10.1371/journal.pone.0073484.t002

showed statistically significant poor prognoses (P = 9.6e-6, Figure 5B). Three SNVs in the ATM gene were significantly enriched in the the phosphatidylinositol 3-/4-kinase catalytic domain (P = 0.014). ATM senses DNA damage and phosphorylates TP53, which, in turn, invokes various cellular responses, such as DNA repair, growth arrest and apoptosis, and collectively prevents cancer progression (Figure S11 in File S1) [43,44].

We also examined whether other frequently mutated genes were associated with better or worse prognoses. We found that patients with PAPPA2 mutations showed prolonged survival times (P = 0.026, Figure 5C and D). PAPPA2 proteolyzes IGFBP5 [45,46], which is an inhibitory factor for IGFs [47]. Mutations in the PAPPA2 gene may result in the accumulation of IGFBP5, and the resulting decrease in IGF signaling may impair the proliferation of cancer cells [48]. Again, it should be noted that for both the ATM and PAPPA2 genes, the statistical significance of the prognostic difference persisted both before (black line) and after (red line) the remaining germline

mutations were removed, which was validated by Sanger sequencing (Figure 5B, D and Table S10 in File S1).

Conclusions

We have identified and characterized the SNVs in lung adenocarcinoma in a Japanese population. Further biological evaluations of the discovered SNVs will be described elsewhere. In particular, information of transcriptome and epigenome should be important for further analyses of cancer genomes, as they would shed new lights on the cancer biology (Table S1) [49]. In this study, we also presented a useful approach for the analysis of cancer exomes, without the need to sequence the normal tissue counterpart. We believe that the approach not only lowers the barriers in cost, time and data fidelity in the exome analysis, but also enables exome analysis of archive samples, for which normal tissue counterparts are not always available.

Materials and Methods

Ethics statement

All of the samples were collected by following the protocol (and written informed consent) which were approved by Ethical Committee in National Cancer Center, Japan (Correspondence to: Katsuya Tsuchihara; ktsuchih@east.ncc.go.jp).

### Case selection and DNA preparation

All of the tissue materials were obtained from Japanese lung adenocarcinoma patients with the appropriate informed consent. Surgically resected primary lung adenocarcinoma samples with lengthwise dimensions in excess of 3 cm were selected. Data on the 52 patients who had relapses and other clinical information about the 97 cases are shown in Table S11 in File **S1**. All 97 cancer and normal tissues were extracted from methanol-fixed samples by laser capture microdissection. DNA purification was performed using an EZ1 Advanced XL Robotic workstation with EZ1 DNA Tissue Kits (Qiagen).

Whole-exome sequencing

Using 1 µg of isolated DNA, we prepared exome-sequencing libraries using the SureSelect Target Enrichment System (Agilent Technologies) according to the manufacturer's protocol. The captured DNA was sequenced by the illumina Genome Analyzer IIx platform (Illumina), yielding 76-base paired-end reads.

Somatic SNV detection

The methods that were used to detect the SNVs, including BWA, SAMtools [50] and GATK, are shown in Figure S2 in File S1. Using data from NCBI dbSNP build 132 and one Japanese genome [51], major germline SNVs were excluded. In addition, rare germline SNVs were discarded using 97 exomes from normal tissue counterparts, 73 Japanese exomes provided from the 1000 Genomes Project (the phase1 exome data, 20110521) and 48 in-house Japanese exomes. We also validated a portion of the SNV datasets by the Sanger

A

○ 97 Japanese
◌ 188 Caucasians

B
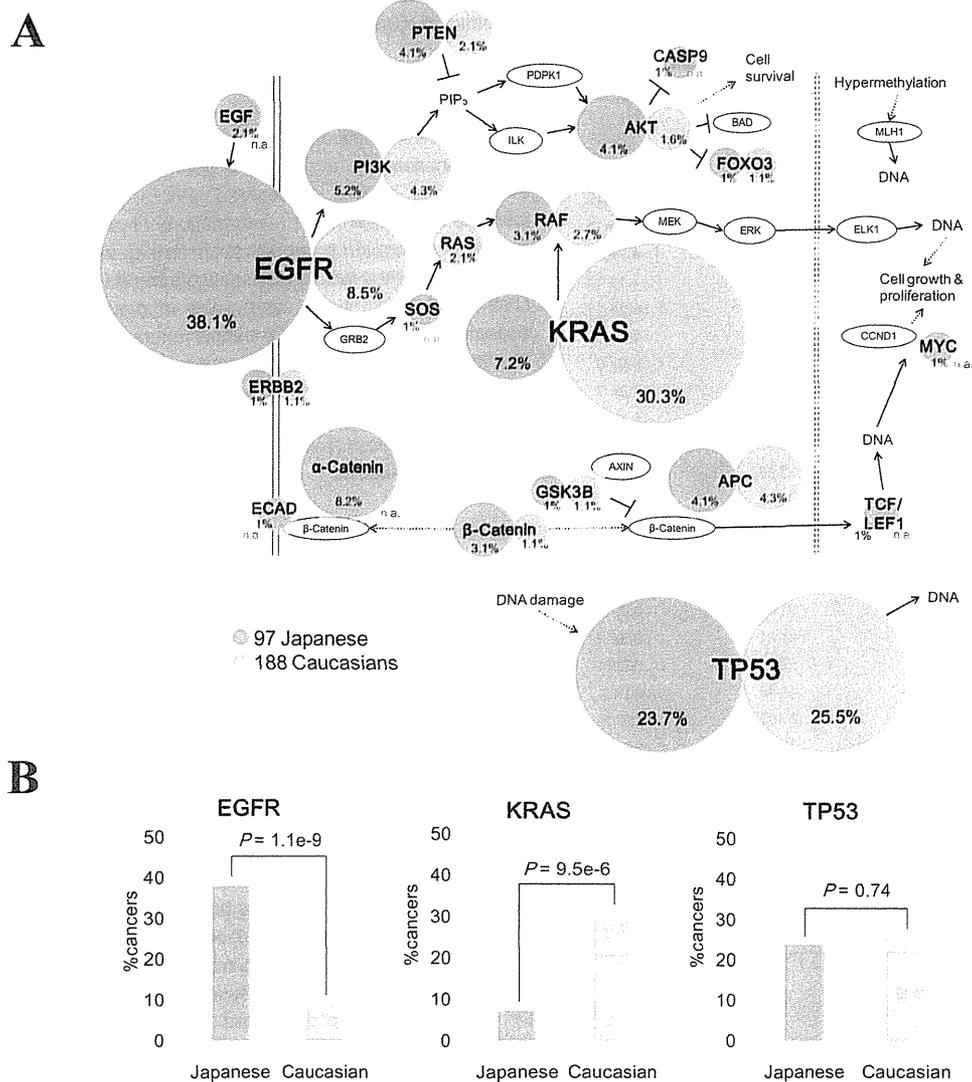
Fig. 2

Figure 2. The EGFR/Ras pathways in Japanese and Caucasian populations. (A) Mutation patterns in the endometrial cancer pathway that was detected in the enrichment analysis are shown. The size of the circle represents the population of the cancers harboring the SNVs in the corresponding gene (percentage is also shown in the margin). SNVs in this study and the external dataset in Caucasian populations are shown in red and blue circles, respectively. n.a.: mutation frequencies were not available. (B) Comparison of mutation ratio of EGFR, KRAS and TP53 genes among both datasets. The p-values were calculated by two-sample test for equality of proportions.

doi: 10.1371/journal.pone.0073484.g002

sequencing of cancer tissues and their normal tissue counterparts (Figure S12 in File S1).

Identification of highly mutated genes

We detected genes which were significantly enriched with SNVs by calculating the expected number of cancers with SNVs in the gene. The length of total CDS regions was represented in N (approximately 30.8 M bases). When one

patient harbored total of m SNVs, the probability that the patient harbors SNVs in the gene t (length: n) was calculated as P:

$$P_{m,t,n} = 1 - \left(1 - \frac{m}{N}\right)^n$$

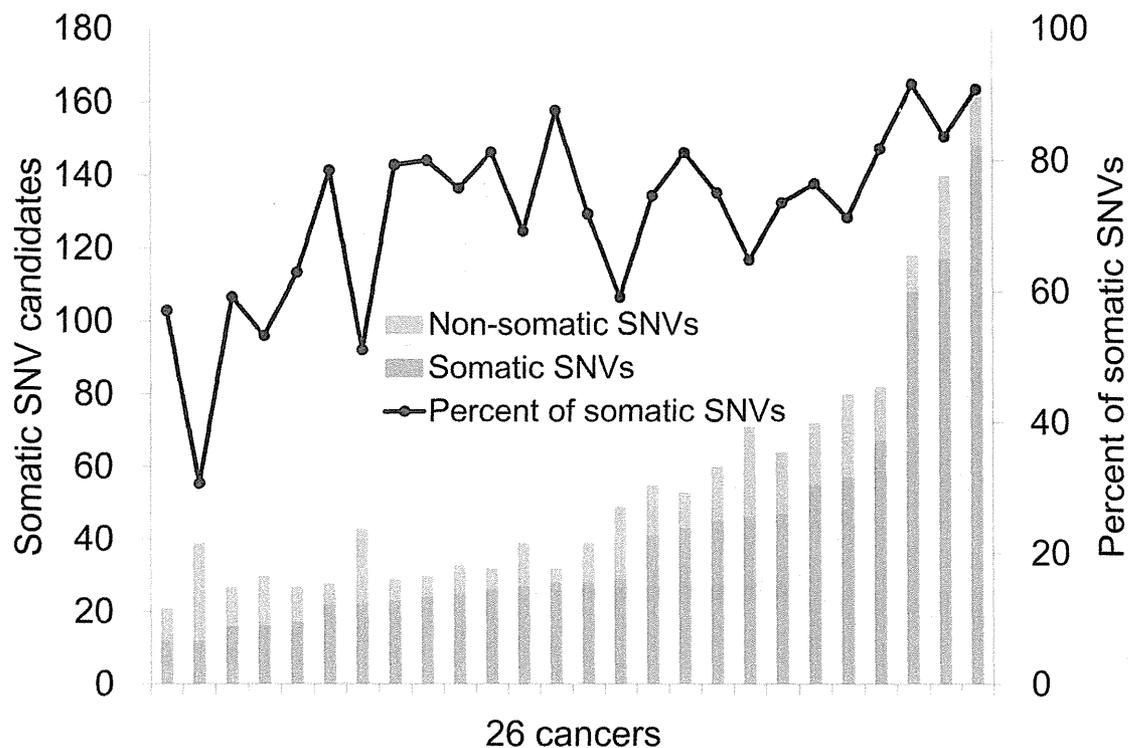The sum of P in 97 cancers was represented in the expected number of cancers with SNVs in the gene t. The p-values of the

Figure 3. Fidelity of the germline SNV detection in cancer exome analysis. Somatic SNV candidates were identified by using 26 cancer exomes and each normal counterpart. Correct somatic SNVs and false positives were shown in pink and blue bars, respectively. The 26 cancers used for the analysis were sorted by the increasing total number of SNVs (x-axis).
doi: 10.1371/journal.pone.0073484.g003

observed number were calculated by the Poisson probability function using R ppois.

Statistical approach to enrichment analyses

To examine the enrichment of mutations in functional protein domains, we mapped the SNVs to domains using InterProScan [52] and assigned them to the Catalogue of Somatic Mutations in Cancer (COSMIC). We analyzed the enrichment of the SNVs in the same domains as the mutations that were provided by the COSMIC. The p-values for the observed mutations in these domains were calculated using their hypergeometric distributions (R phyper). Briefly, the domains in which the SNVs were enriched statistically significantly than the expected number of SNVs in the given length of the domain were selected. For estimating the expected number, the total number of the SNVs belonging to the gene was divided by the gene length. For this analysis, we used genes harboring five or more SNVs in the coding region and three or more SNVs in the domain.

We assigned SNVs to pathways as described by the Kyoto Encyclopedia of Genes and Genomes (KEGG) and calculated the enrichments of the SNVs in the pathways. The mutation rate M represented the ratio of the average number of mutated genes to the total number of genes (17,175) that were used in our study. The expected value for the number of cancers with SNVs in pathway t was designated λ and calculated from the mutation rate M and the number of genes in the pathway n as follows:

$$\lambda_{t,n} = \left\{ 1 - (1-M)^n \right\} \times 97$$

The p-value for the observed number of cancers with SNVs in pathway t was calculated by the Poisson probability function using R ppois.
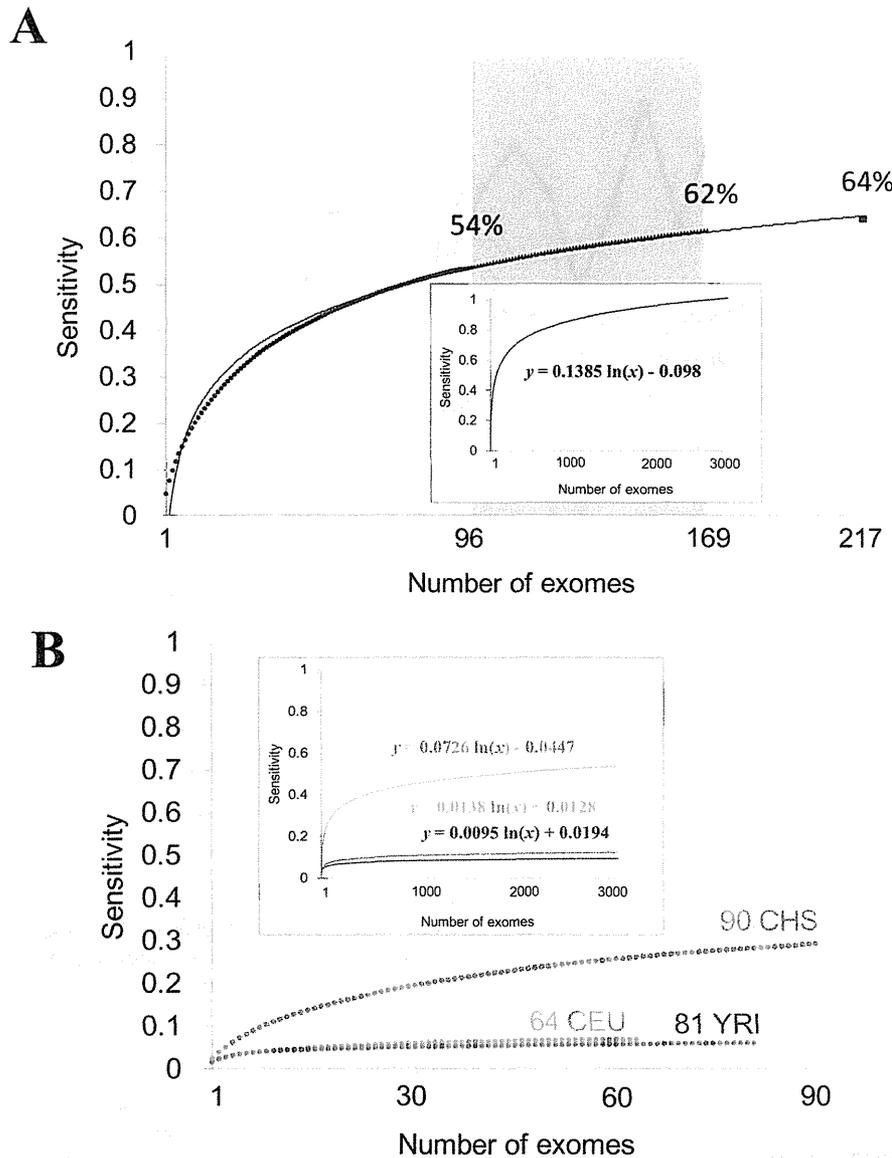
Figure 4. Discriminative powers of detecting germline SNVs using external references. (A) The power of detecting germline SNVs considering mutual overlap between other Japanese individuals. Sensitivity represents the proportion of germline SNVs correctly detected. The datasets used to exclude the germline SNVs are shown on the x axis. The inset represents the extrapolation of the graph. Fitting curve of the graph is also shown. (B) Discriminative powers of three different ethnic groups for the germline SNVs in 97 Japanese cancers. Sensitivities for detecting germline SNVs are shown by the following colors; green: Chinese; purple: Yoruba; orange: Caucasian.

Estimate of discriminative power for exclusion of germline SNVs by considering mutual overlaps

We estimated the discriminative power for the exclusion of germline SNVs by considering those from other non-cancerous exomes. Germline SNVs from 97 paired tumor-normal exomes were used as reference datasets. Up to 217 samples (96 normal tissue exomes from others and 121 additional Japanese exomes) were randomly selected, and their sensitivities and specificities for detecting the germline SNVs were detected by taking the averages of either all of the combinations or a subset of approximately 10,000 combinations. We also estimated the discriminative power with
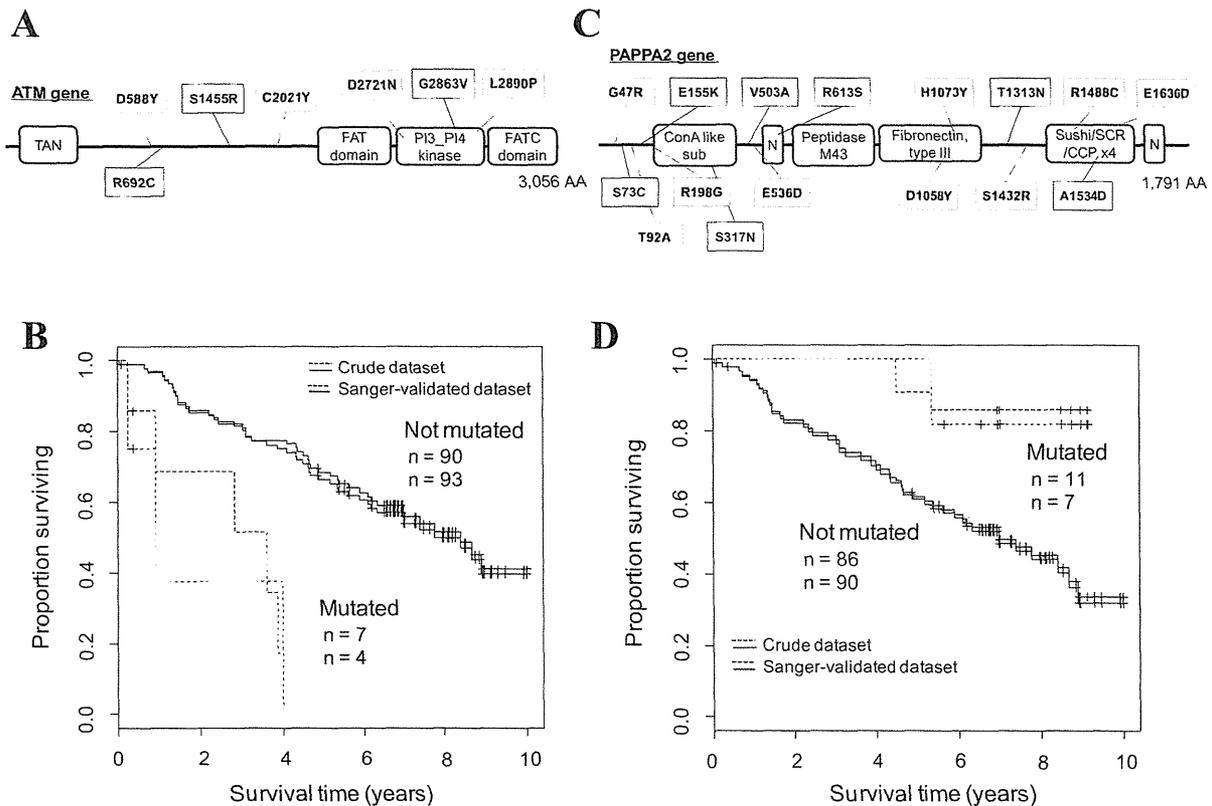
Fig. 5

Figure 5. Identification of the putative prognosis-related genes. (A) SNVs in the ATM gene. The SNVs that were identified in the initial screening and those remaining after the Sanger sequencing validation of the normal-tissue counterpart were shown in black and red, respectively. TAN: Telomere-length maintenance and DNA damage repair; PI3_PI4 kinase: Phosphatidylinositol 3-/4-kinase, catalytic. (B) Survival analysis of patients with and without ATM SNVs. The datasets before and after the Sanger sequencing validation are represented by black and red lines, respectively. Statistical significance was calculated using a log-rank test ($P < 0.05$). Note that the survival differences for individuals with SNVs in the non-Sanger-validated dataset were significant before the Sanger validation. (C, D) Results of a similar analysis as that described in A and B for the PAPPA2 gene. In this case, the patients with the SNVs showed better prognoses. ConA like sub: Concanavalin A-like lectin/glucanase, subgroup; N: Notch dimain; Peptidase M43: Peptidase M43, pregnancy-associated plasma-A.

Table 3. Comparison of the results in the enrichment analyses between the crude and refined dataset.

	Number of identified genes/pathways		
	Crude[*]	Refined[†]	Overlap[‡]
Genes	16	11	9
Pathways	23	26	19

[*] Identified using the crude dataset.

[†] Identified using the refined dataset.

[‡] Significant in both crude and refined datasets.

data from the 1000 Genomes Project for four ethnic groups (73 JPT, 90 CHS, 81 YRI and 64 CEU) using similar trials. Whole-exome sequences (the phase1 exome data, 20110521) were obtained from the ftp site in the 1000 Genomes Project.

Kaplan-Meier curves

The Kaplan-Meier method was used to test the relations of the observed mutations to survival time, and calculations were performed using the R software package. Changes in survival rates that were correlated with SNVs were examined using the log-rank test (R survdiff).

Data access

Full raw datasets will be shared with researchers upon request. The information of somatic mutations at the respective genomic coordinates has been provided in Table S2.

Supporting Information

File S1.   Figures S1 to S12 and Tables S3 to S11 are included.
(PDF)

Table S1.   The comparison of our dataset with the other different study. We provided the comparison of our dataset with the genes identified in the other different study with transcriptome and epigenome data in lung cancers.
(XLSX)

Table S2.   The list of somatic mutations identified from the refined dataset. All mutations described in this table are somatic and non-synonymous mutations.

(XLSX)

Author Contributions

Conceived and designed the experiments: KT YS HE KG SS. Performed the experiments: SM YY AK KM MS. Analyzed the data: AS YS KT. Contributed reagents/materials/analysis tools: KG KT. Wrote the manuscript: AS KT YS.

References

1. The 1000 Genomes Project Consortium (2010) A map of human genome variation from population-scale sequencing. Nature 467: 1061-1073. doi:10.1038/nature09534. PubMed: 20981092.
2. The 1000 Genomes Project Consortium (2012) An integrated map of genetic variation from 1,092 human genomes. Nature 491: 56-65. doi:10.1038/nature11632. PubMed: 23128226.
3. Choi M, Scholl UI, Ji W, Liu T, Tikhonova IR et al. (2009) Genetic diagnosis by whole exome capture and massively parallel DNA sequencing. Proc Natl Acad Sci U S A 106: 19096-19101. doi:10.1073/pnas.0910672106. PubMed: 19861545.
4. Ng SB, Turner EH, Robertson PD, Flygare SD, Bigham AW et al. (2009) Targeted capture and massively parallel sequencing of 12 human exomes. Nature 461: 272-276. doi:10.1038/nature08250. PubMed: 19684571.
5. Clark MJ, Chen R, Lam HY, Karczewski KJ, Chen R et al. (2011) Performance comparison of exome DNA sequencing technologies. Nat Biotechnol 29: 908-914. doi:10.1038/nbt.1975. PubMed: 21947028.
6. Bamshad MJ, Ng SB, Bigham AW, Tabor HK, Emond MJ et al. (2011) Exome sequencing as a tool for Mendelian disease gene discovery. Nat Rev Genet 12: 745-755. doi:10.1038/nrg3031. PubMed: 21946919.
7. Ng SB, Buckingham KJ, Lee C, Bigham AW, Tabor HK et al. (2010) Exome sequencing identifies the cause of a mendelian disorder. Nat Genet 42: 30-35. doi:10.1038/ng.499. PubMed: 19915526.
8. Biesecker LG (2010) Exome sequencing makes medical genomics a reality. Nat Genet 42: 13-14. doi:10.1038/ng0110-13. PubMed: 20037612.
9. Louis-Dit-Picard H, Barc J, Trujillano D, Miserey-Lenkei S, Bouatia-Naji N et al. (2012) KLHL3 mutations cause familial hyperkalemic hypertension by impairing ion transport in the distal nephron. Nat Genet.
10. Sherry ST, Ward MH, Kholodov M, Baker J, Phan L et al. (2001) dbSNP: the NCBI database of genetic variation. Nucleic Acids Res 29: 308-311. doi:10.1093/nar/29.1.308. PubMed: 11125122.
11. Futreal PA, Coin L, Marshall M, Down T, Hubbard T et al. (2004) A census of human cancer genes. Nat Rev Cancer 4: 177-183. doi:10.1038/nrc1299. PubMed: 14993899.
12. International Cancer Genome Consortium (2010) International network of cancer genome projects. Nature 464: 993-998. doi:10.1038/nature08987. PubMed: 20393554.
13. Totoki Y, Tatsuno K, Yamamoto S, Arai Y, Hosoda F et al. (2011) High-resolution characterization of a hepatocellular carcinoma genome. Nat Genet 43: 464-469. doi:10.1038/ng.804. PubMed: 21499249.
14. Jones DT, Jäger N, Kool M, Zichner T, Hutter B et al. (2012) Dissecting the genomic complexity underlying medulloblastoma. Nature 488: 100-105. doi:10.1038/nature11284. PubMed: 22832583.

15. The Cancer Genome Atlas Research Network (2011) Integrated genomic analyses of ovarian carcinoma. Nature 474: 609-615. doi:10.1038/nature10166. PubMed: 21720365.
16. Stephens PJ, Tarpey PS, Davies H, Van Loo P, Greenman C et al. (2012) The landscape of cancer genes and mutational processes in breast cancer. Nature 486: 400-404. PubMed: 22722201.
17. The Cancer Genome Atlas Research Network (2012) Comprehensive genomic characterization of squamous cell lung cancers. Nature.
18. The Cancer Genome Atlas Research Network (2012) Comprehensive molecular characterization of human colon and rectal cancer. Nature 487: 330-337. doi:10.1038/nature11252. PubMed: 22810696.
19. Imielinski M, Berger AH, Hammerman PS, Hernandez B, Pugh TJ et al. (2012) Mapping the hallmarks of lung adenocarcinoma with massively parallel sequencing. Cell 150: 1107-1120. doi:10.1016/j.cell.2012.08.029. PubMed: 22980975.
20. Davies H, Hunter C, Smith R, Stephens P, Greenman C et al. (2005) Somatic mutations of the protein kinase gene family in human lung cancer. Cancer Res 65: 7591-7595. PubMed: 16140923.
21. Ding L, Getz G, Wheeler DA, Mardis ER, McLellan MD et al. (2008) Somatic mutations affect key pathways in lung adenocarcinoma. Nature 455: 1069-1075. doi:10.1038/nature07423. PubMed: 18948947.
22. Kan Z, Jaiswal BS, Stinson J, Janakiraman V, Bhatt D et al. (2010) Diverse somatic mutation patterns and pathway alterations in human cancers. Nature 466: 869-873. doi:10.1038/nature09208. PubMed: 20668451.
23. Forbes SA, Bhamra G, Bamford S, Dawson E, Kok C et al. (2008) The Catalogue of Somatic Mutations in Cancer (COSMIC). Curr Protoc Hum Genet Chapter 10: Unit 10.11: PubMed: 18428421
24. Forbes SA, Bindal N, Bamford S, Cole C, Kok CY et al. (2011) COSMIC: mining complete cancer genomes in the Catalogue of Somatic Mutations in Cancer. Nucleic Acids Res 39: D945-D950. doi:10.1093/nar/gkq929. PubMed: 20952405.
25. Li H, Durbin R (2009) Fast and accurate short read alignment with Burrows-Wheeler transform. Bioinformatics 25: 1754-1760. doi:10.1093/bioinformatics/btp324. PubMed: 19451168.
26. McKenna A, Hanna M, Banks E, Sivachenko A, Cibulskis K et al. (2010) The Genome Analysis Toolkit: a MapReduce framework for analyzing next-generation DNA sequencing data. Genome Res 20: 1297-1303. doi:10.1101/gr.107524.110. PubMed: 20644199.
27. DePristo MA, Banks E, Poplin R, Garimella KV, Maguire JR et al. (2011) A framework for variation discovery and genotyping using next-generation DNA sequencing data. Nat Genet 43: 491-498. doi:10.1038/ng.806. PubMed: 21478889.
28. Welch HC, Coadwell WJ, Ellson CD, Ferguson GJ, Andrews SR et al. (2002) P-Rex1, a PtdIns(3,4,5)P3- and Gbetagamma-regulated guanine-nucleotide exchange factor for Rac. Cell 108: 809-821. doi:10.1016/S0092-8674(02)00663-3. PubMed: 11955434.

29. Rosenfeldt H, Vázquez-Prado J, Gutkind JS (2004) P-REX2, a novel PI-3-kinase sensitive Rac exchange factor. FEBS Lett 572: 167-171. doi:10.1016/j.febslet.2004.06.097. PubMed: 15304342.

30. Das B, Shu X, Day GJ, Han J, Krishna UM et al. (2000) Control of intramolecular interactions between the pleckstrin homology and Dbl homology domains of Vav and Sos1 regulates Rac binding. J Biol Chem 275: 15074-15081. doi:10.1074/jbc.M907269199. PubMed: 10748082.

31. Hill K, Krugmann S, Andrews SR, Coadwell WJ, Finan P et al. (2005) Regulation of P-Rex1 by phosphatidylinositol (3,4,5)-trisphosphate and Gbetagamma subunits. J Biol Chem 280: 4166-4173. PubMed: 15545267.

32. Chhatriwala MK, Betts L, Worthylake DK, Sondek J (2007) The DH and PH domains of Trio coordinately engage Rho GTPases for their efficient activation. J Mol Biol 368: 1307-1320. doi:10.1016/j.jmb. 2007.02.060. PubMed: 17391702.

33. Sosa MS, Lopez-Haber C, Yang C, Wang H, Lemmon MA et al. (2010) Identification of the Rac-GEF P-Rex1 as an essential mediator of ErbB signaling in breast cancer. Mol Cell 40: 877-892. doi:10.1016/j.molcel. 2010.11.029. PubMed: 21172654.

34. Kanehisa M, Goto S, Furumichi M, Tanabe M, Hirakawa M (2010) KEGG for representation and analysis of molecular networks involving diseases and drugs. Nucleic Acids Res 38: D355-D360. doi: 10.1093/nar/gkp896. PubMed: 19880382.

35. Hecht JL, Mutter GL (2006) Molecular and pathologic aspects of endometrial carcinogenesis. J Clin Oncol 24: 4783-4791. doi:10.1200/ JCO.2006.06.7173. PubMed: 17028294.

36. Li C, Fang R, Sun Y, Han X, Li F et al. (2011) Spectrum of oncogenic driver mutations in lung adenocarcinomas from East Asian never smokers. PLOS ONE 6: e28204. doi:10.1371/journal.pone.0028204. PubMed: 22140546.

37. Shigematsu H, Lin L, Takahashi T, Nomura M, Suzuki M et al. (2005) Clinical and biological features associated with epidermal growth factor receptor gene mutations in lung cancers. J Natl Cancer Inst 97: 339-346. doi:10.1093/jnci/dji055. PubMed: 15741570.

38. Sharma SV, Bell DW, Settleman J, Haber DA (2007) Epidermal growth factor receptor mutations in lung cancer. Nat Rev Cancer 7: 169-181. doi:10.1038/nrc2088. PubMed: 17318210.

39. Bos JL (1989) ras oncogenes in human cancer: a review. Cancer Res 49: 4682-4689. PubMed: 2547513.

40. Degen M, Brellier F, Kain R, Ruiz C, Terracciano L et al. (2007) Tenascin-W is a novel marker for activated tumor stroma in low-grade human breast cancer and influences cell behavior. Cancer Res 67: 9169-9179. doi:10.1158/0008-5472.CAN-07-0666. PubMed: 17909022.

41. Degen M, Brellier F, Schenk S, Driscoll R, Zaman K et al. (2008) Tenascin-W, a new marker of cancer stroma, is elevated in sera of

colon and breast cancer patients. Int J Cancer 122: 2454-2461. doi: 10.1002/ijc.23417. PubMed: 18306355.

42. Brellier F, Martina E, Degen M, Heuzé-Vourc'h N, Petit A et al. (2012) Tenascin-W is a better cancer biomarker than tenascin-C for most human solid tumors. BMC Clin Pathol 12: 14. doi: 10.1186/1472-6890-12-14. PubMed: 22947174.

43. Dasika GK, Lin SC, Zhao S, Sung P, Tomkinson A et al. (1999) DNA damage-induced cell cycle checkpoints and DNA strand break repair in development and tumorigenesis. Oncogene 18: 7883-7899. PubMed: 10630641.

44. Bartkova J, Horejsi Z, Koed K, Kramer A, Tort F et al. (2005) DNA damage response as a candidate anti-cancer barrier in early human tumorigenesis. Nature 434: 864-870. doi:10.1038/nature03482. PubMed: 15829956.

45. Yan X, Baxter RC, Firth SM (2010) Involvement of pregnancy-associated plasma protein-A2 in insulin-like growth factor (IGF) binding protein-5 proteolysis during pregnancy: a potential mechanism for increasing IGF bioavailability. J Clin Endocrinol Metab 95: 1412-1420. doi:10.1210/jc.2009-2277. PubMed: 20103653.

46. Overgaard MT, Boldt HB, Laursen LS, Sottrup-Jensen L, Conover CA et al. (2001) Pregnancy-associated plasma protein-A2 (PAPP-A2), a novel insulin-like growth factor-binding protein-5 proteinase. J Biol Chem 276: 21849-21853. doi:10.1074/jbc.M102191200. PubMed: 11264294.

47. Shimasaki S, Shimonaka M, Zhang HP, Ling N (1991) Identification of five different insulin-like growth factor binding proteins (IGFBPs) from adult rat serum and molecular cloning of a novel IGFBP-5 in rat and human. J Biol Chem 266: 10646-10653. PubMed: 1709938.

48. Su Y, Wagner ER, Luo Q, Huang J, Chen L et al. (2011) Insulin-like growth factor binding protein 5 suppresses tumor growth and metastasis of human osteosarcoma. Oncogene 30: 3907-3917. doi: 10.1038/onc.2011.97. PubMed: 21460855.

49. Huang T, Jiang M, Kong X, Cai YD (2012) Dysfunctions associated with methylation, microRNA expression and gene expression in lung cancer. PLOS ONE 7: e43441. doi:10.1371/journal.pone.0043441. PubMed: 22912875.

50. Li H, Handsaker B, Wysoker A, Fennell T, Ruan J et al. (2009) The Sequence Alignment/Map format and SAMtools. Bioinformatics 25: 2078-2079. doi:10.1093/bioinformatics/btp352. PubMed: 19505943.

51. Fujimoto A, Nakagawa H, Hosono N, Nakano K, Abe T et al. (2010) Whole-genome sequencing and comprehensive variant analysis of a Japanese individual using massively parallel sequencing. Nat Genet 42: 931-936. doi:10.1038/ng.691. PubMed: 20972442.

52. Quevillon E, Silventoinen V, Pillai S, Harte N, Mulder N et al. (2005) InterProScan: protein domains identifier. Nucleic Acids Res 33: W116-W120. doi:10.1093/nar/gni118. PubMed: 15980438.

Identification of a lung adenocarcinoma cell line with CCDC6-RET fusion gene and the effect of RET inhibitors *in vitro* and *in vivo*

Makito Suzuki,[1,2,11] Hideki Makinoshima,[1,11] Shingo Matsumoto,[1,3] Ayako Suzuki,[4] Sachiyo Mimaki,[1] Koutatsu Matsushima,[1,2] Kiyotaka Yoh,[3] Koichi Goto,[3] Yutaka Suzuki,[4] Genichiro Ishii,[5] Atsushi Ochiai,[5] Koji Tsuta,[6] Tatsuhiro Shibata,[7] Takashi Kohno,[8] Hiroyasu Esumi[9] and Katsuya Tsuchihara[1,2,10]

[1]Division of Translational Research, Research Center for Innovative Oncology, National Cancer Center Hospital East, Kashiwa, Chiba; [2]Department of Integrated Biosciences, Graduate School of Frontier Sciences, The University of Tokyo, Kashiwa, Chiba; [3]Division of Thoracic Oncology, National Cancer Center Hospital East, Kashiwa, Chiba; [4]Department of Medical Genome Sciences, Graduate School of Frontier Sciences, The University of Tokyo, Kashiwa, Chiba; [5]Division of Pathology, Research Center for Innovative Oncology, National Cancer Center Hospital East, Kashiwa, Chiba; [6]Division of Pathology and Clinical Laboratories, National Cancer Center Hospital, Tokyo; Divisions of [7]Cancer Genomics; [8]Genome Biology, National Cancer Center Research Institute, Tokyo; [9]National Cancer Center Hospital East, Kashiwa, Chiba, Japan

Rearrangements of the proto-oncogene *RET* are newly identified potential driver mutations in lung adenocarcinoma (LAD). However, the absence of cell lines harboring *RET* fusion genes has hampered the investigation of the biological relevance of RET and the development of RET-targeted therapy. Thus, we aimed to identify a *RET* fusion positive LAD cell line. Eleven LAD cell lines were screened for *RET* fusion transcripts by reverse transcription-polymerase chain reaction. The biological relevance of the *CCDC6-RET* gene products was assessed by cell growth, survival and phosphorylation of ERK1/2 and AKT with or without the suppression of RET expression using RNA interference. The efficacy of RET inhibitors was evaluated *in vitro* using a culture system and in an *in vivo* xenograft model. Expression of the *CCDC6-RET* fusion gene in LC-2/ad cells was demonstrated by the mRNA and protein levels, and the genomic break-point was confirmed by genomic DNA sequencing. Mutations in *KRAS* and *EGFR* were not observed in the LC-2/ad cells. CCDC6-RET was constitutively active, and the introduction of a siRNA targeting the *RET 3′* region decreased cell proliferation by downregulating RET and ERK1/2 phosphorylation. Moreover, treatment with RET-inhibitors, including vandetanib, reduced cell viability, which was accompanied by the downregulation of the AKT and ERK1/2 signaling pathways. Vandetanib exhibited anti-tumor effects in the xenograft model. Endogenously expressing CCDC6-RET contributed to cell growth. The inhibition of kinase activity could be an effective treatment strategy for LAD. LC-2/ad is a useful model for developing fusion RET-targeted therapy. (*Cancer Sci* 2013; 104: 896–903)

L ung cancer is the most common cause of cancer death worldwide.[1] The identification of oncogenic driver genes is to select the increasing number of small molecule inhibitors targeting these gene products.[2,3] In particular, in lung adenocarcinoma (LAD), the most dominant histological subtype of lung cancer, the application of kinase inhibitors for cases with specific gene alterations has been successful, that is, gefitinib and erlotinib for *EGFR* mutation-positive cases and crizotinib for *ALK* fusion-positive cases.[4–7] Furthermore, accumulating evidence has demonstrated somatic mutations and rearrangements of potential oncogenes, including *BRAF*, *ERBB2* and *ROS1*, in LAD.[8–10]

RET is one of the newest LAD driver genes.[11–15] *RET* gene is located on chromosome 10 and encodes a receptor tyrosine

kinase,[16,17] and the oncogenic potential of this gene product has been suggested in several tumors, including thyroid cancer.[18–20] Recently, five independent groups identified aberrant fusion genes, *KIF5B-RET* and *CCDC6-RET* in clinical samples of LAD.[11–15] Ectopically expressed RET fusion products afforded NIH3T3 cells with anchorage-independent growth and tumorigenicity in nude mice.[11,14] Furthermore, KIF5B-RET-expressing H1299 cells exhibited growth factor-independent growth.[11] These findings strongly suggest the oncogenic activity of RET fusion products and also suggest the potential therapeutic efficacy of multi-kinase inhibitor targeting of RET using the abovementioned cells. However, LAD-derived cell lines harboring *RET* fusion genes had not been identified. Recently, Matsubara *et al.*[21] screened LAD cell lines that were sensitive to a RET inhibitor vandetanib and found a *CCDC6-RET* fusion gene-harboring cell line, LC-2/ad.

We have independently screened cell lines established from Japanese LAD samples by RT-PCR and found that LC-2/ad cells expressed the *CCDC6-RET* fusion gene product. We further examined whether LC-2/ad cells depend on RET fusion-mediated signaling. In addition, the antitumor effect of RET inhibitors in LC-2/ad cells was evaluated *in vitro* and *in vivo*.

Materials and Methods

Complete materials and methods were described in the supplementary information (Data S1. Materials and Methods).

Purchased materials. Cell lines were purchased from RIKEN Bio Resource Center, the Immuno-Biological Laboratories (Fujioka, Japan) and American Type Culture Collection. Procedures for western blotting was previously described.[22] Primary antibodies specific for RET and phospho-RET Tyr-905 were purchased from Epitomics (Burlingame, CA, USA) and Cell Signaling Technologies (Danvers, MA, USA), respectively. RET-targeting siRNA was purchased from Life Technologies (Carlsbad, CA, USA). Gefitinib, sunitinib malate and sorafenib were purchased from Santa Cruz Biotechnology (Dallas, TX, USA), Sigma-Aldrich (St. Louis, MO, USA) and Toronto Research Chemicals (Toronto, ON, Canada),

---

[10]To whom correspondence should be addressed.
E-mail: ktsuchih@east.ncc.go.jp
[11]These authors contributed equally to this work.

respectively. Vandetanib, AZD6244 and BEZ235 were purchased from Selleck (Houston, TX, USA).

Multiplex RT-PCR. Reported *KIF5B/CCDC6-RET* fusion variants were detected by multiplex RT-PCR according to the procedures described elsewhere.[11,14]

Genomic DNA sequencing. LC-2/ad DNA was captured with custom hybridization probes targeting *CCDC6* intron 1 and *RET* whole gene (Agilent) followed by parallel sequencing on the MiSeq system (Illumina).

Real-time RT-PCR. Procedures for real-time RT-PCR was previously described.[22] The PCR primers used in the present study are shown in Table S1.

In vivo studies. LC2/ad cells at 5.0×10^6 were subcutaneously inoculated to 8-week-old athymic nude mice (Clea Japan).[23] Vandetanib was administered once daily as a homogeneous suspension by oral gavage at a dosage of 50 mg/kg body weight.[24] The tumor volume was calculated as the product of a scaling factor ($\pi/6$) and the tumor length, width and height.[22] The study was approved by the Institutional Ethics Review Committee for animal experiments at the National Cancer Center.

Immunohistochemical analysis. The procedure for hematoxylin eosin staining and immunohistochemical (IHC) was previously described.[22,25]

Microarray analysis. Background information of clinical samples was described in a previous report.[26] The study was approved by the Institutional Review Boards of the National Cancer Center. Total RNA was analyzed using Affymetrix (Santa Clara, CA, USA) U133Plus2.0 arrays. The data were processed by the MAS5 algorithm, and the mean expression level of a total of 54 675 probes was adjusted to 1000 for each sample.

Results

Identification of the *CCDC6-RET* fusion gene in a Japanese LAD cell line. To identify *RET* fusion-derived mRNA expression in human LAD cell lines, all reported *KIF5B-RET* and *CCDC6-RET* gene products were screened by multiplex RT-PCR in 11 cell lines derived from Japanese patients. LC-2/ad cells were found to express *CCDC6-RET* mRNA at significantly higher levels, whereas the other cell lines did not exhibit any fusion gene products (Fig. 1a). The expressed fusion *RET* product was sequenced, and an in-frame fusion of *CCDC6* exon 1 and *RET* exon 12, which was identical to the previously reported *CCDC6-RET* fusion products, was identified (Fig. 1b).[14] We then identified a breakpoint of chromosome 10 by retrieving genomic DNA fragments, including the entire *RET* gene and intron 1 of *CCDC6*, by target capture system followed by parallel sequencing. The identified break-point between *CCDC6* intron 1 and *RET* exon 11 was confirmed by Sanger sequencing (Fig. 1b). Quantitative RT-PCR revealed that the expression of 3' end of *RET* was increased comparable to that of *CCDC6*, whereas the transcript level of the 5' end of *RET* was significantly lower (Fig. 1c). Consistent with the amount of transcript, western blotting using an antibody recognizing the C-terminus of RET isoform 2 detected a 60-kDa specific band equivalent to
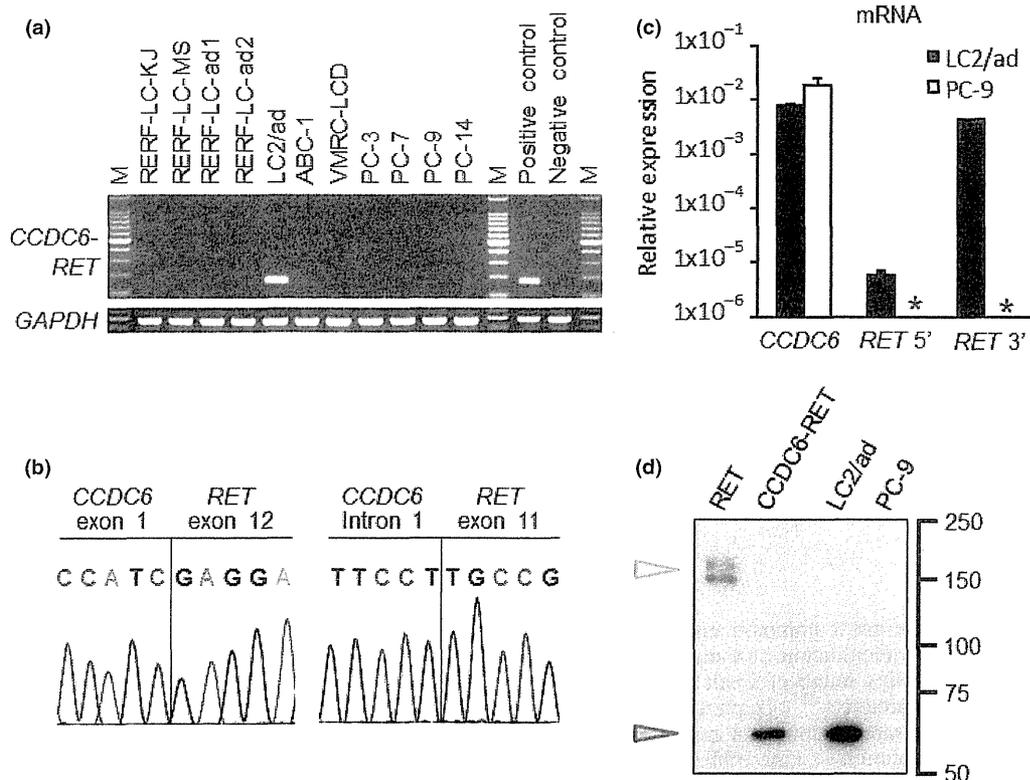
Fig. 1. Identification of the *CCDC6-RET* fusion gene. (a) Detection of *RET* fusion transcripts in lung adenocarcinoma (LAD) cell lines by multiplex reverse transcription-polymerase chain reaction (RT-PCR). (b) Sanger sequencing around the fusion point of the cDNA (left) and the breakpoint of the genomic DNA (right) of *CCDC6-RET* in LC-2/ad cells. (c) 3' region-specific expression of *RET* mRNA in LC-2/ad cells. The 5' or 3' region of *RET* and *CCDC6* cDNA level was normalized to glyceraldehyde 3-phosphate dehydrogenase (*GAPDH*) expression. The data are shown as the mean ± standard deviation (SD) (*n* = 3). Asterisks indicate that mRNA expression were below the level of detection. (d) Specific expression of the CCDC6-RET fusion protein. Whole-cell lysates of LC2/ad and PC-9 cells and HEK293 cells transfected with wild-type RET (RET) or CCDC6-RET expression plasmids were subjected to western blot analysis to detect RET protein isoform 2. The LC-2/ad cells showed an approximately 60-kDa (red arrowhead) but not 170-kDa (blue arrowhead) band.
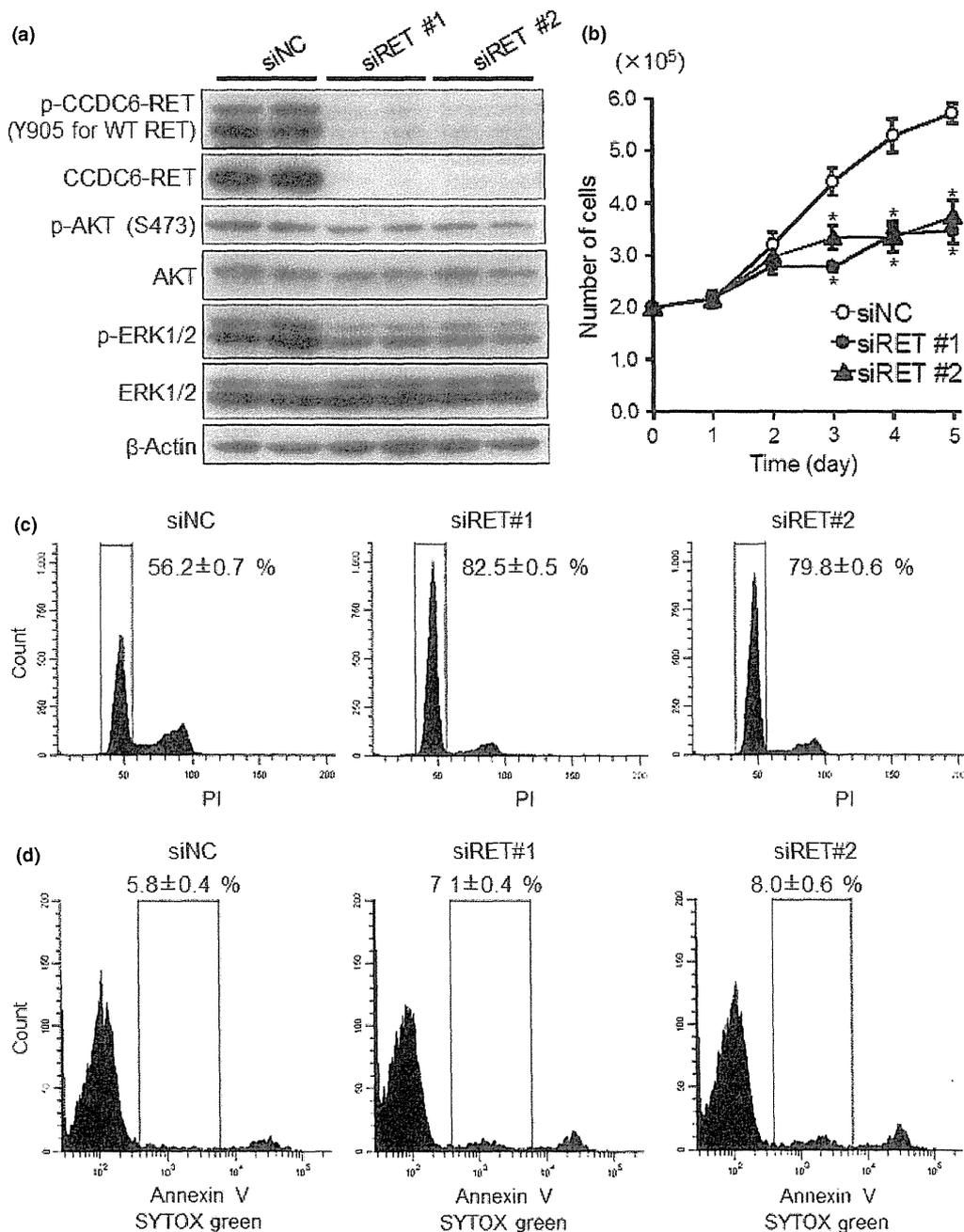
Fig. 2. Suppression of CCDC-RET expression by siRNA in LC-2/ad cells. (a) Western blot analysis of siRET-treated LC-2/ad cells. The siRNA transfected cell lysates were applied to the western blotting. (b) Involvement of RET suppression in cell growth inhibition. LC-2/ad cells transfected with siRNAs were incubated for the indicated times. The data are shown as the mean ± standard deviation (SD) ($n = 4$). *$P < 0.01$ (Student's t-test). (c,d) The DNA ploidy (c) and Annexin V-positive population (d) of siRET-transfected LC-2/ad cells. After 72 h of siRNA transfection, the cells were subjected to DNA ploidy analysis and Annexin V staining. The data are shown as the mean ± SD ($n = 4$).

the estimated size of the fusion protein composed of 503 amino acids (GeneBank BAM36435), whereas no significant signal was detected that approximated the size of wild-type RET, 170-kDa (Fig. 1d).[11] Taken together, we concluded that LC-2/ad cells express CCDC6-RET fusion gene products. KRAS exon 2 and EGFR exon 19 and 21 were examined by Sanger sequencing, but no obvious mutation was confirmed (Fig. S1).

CCDC6-RET-dependent ERK1/2 phosphorylation and the proliferation of LC-2/ad cells. We suppressed RET expression by RNAi to characterize the function of CCDC6-RET in LC-2/ad

cells. For avoiding off-target siRNA effects, two different sequences of siRNA directed against the 3′ region of RET (siRET#1 and #2) and a nontargeting siRNA (siNC) were used. When compared to siNC, a significant reduction in mRNA expression was observed by quantitative RT-PCR detecting the 3′ end of the RET mRNA: 66.5% for siRET#1 and 94.2% for siRET#2 (Fig. S2). Western blot analyses also revealed significant decreases in the expression of CCDC6-RET protein (60-kDa) upon the introduction of siRET#1 and #2 compared to the control siNC in the LC-2/ad cells